2009

Dependence of bubble size and peak rarefractional pressure on maximum bubble response during therapeutic ultrasound histotripsy

Kelsey Jean Carvell
Iowa State University

Dependence of bubble size and peak rarefractional pressure on maximum bubble response during therapeutic ultrasound histotripsy

by

Kelsey Jean Carvell

A thesis submitted to the graduate faculty

in partial fulfillment of the requirements for the degree of

MASTER OF SCIENCE

Major: Electrical Engineering

Program of Study Committee:

Timothy Bigelow, Major Professor

Scott McClure

Viren Amin

Iowa State University

Ames, Iowa

2009

DEDICATION

I dedicate this thesis to my family. My parents, Melanie and Charles Carvell have been incredibly supportive and encouraging. They instilled motivation, self confidence, and a hard work ethic in me from an early age which had brought me to this graduate school and carried me through its courses and requirements. My two little brothers, Robert and Elliot have given perspective and support. They remind daily to set an example. I would also like to dedicate this to my grandmother Adeline. She was raised by her siblings after the death of her mother. In the 1930's she courageously enrolled in college, paying for it on her own, defeating the odds, and even fibbing her age so she would be accepted. As a woman in engineering I hope she can see some of herself in me as I do.

TABLE OF CONTENTS

LIST OF FIGURES……iv
LIST OF TABLES……v
ABSTRACT……vi
ACKNOWLEDGEMENT ……vii
CHAPTER ONE: OVERVIEW…… 1

1.1 Background Therapeutic Ultrasound Work 3
1.2 Background Histotripsy Work 3
1.3 Background Cavitation Work 5
1.4 Research Objective 6
1.5 Thesis Organization 7

CHAPTER TWO: THEORY……8

2.1 Rectified Diffusion 8
2.2 Bubble Dynamics 11
2.3 Cavitation 13

CHAPTER THREE: SIMULATIONS……15

3.1 Simulation Motivation and Code 15
3.2 New Definition of Optimal Seed Size 16
3.3 Equations Solved 20

CHAPTER FOUR: SIMULATION RESULTS……25

4.1 Dependence of Optimal Seed Size 25
4.2 Pressure Threshold 30

CHAPTER FIVE: EXPERIMENTS USING *Ex Vivo* PORCINE LIVER ……32

5.1 Tissue Preparation 32
5.2 Experimental Apparatus 33
5.3 Experimental Results 37

CHAPTER SIX: DISCUSSION……40

APPENDIX A: DERIVATION OF AVERAGE TIME RATE OF CHANGE IN MOLES OF GAS. 45

APPENDIX B: DERIVATION OF RAYLEIGH-PLESSET EQUATION IN TERMS OF BUBBLE RADIUS……50

APPENDIX C: DERIVATION OF GILMORE FORMULATION FOR BUBBLE DYNAMICS 52

APPENDIX D: DERIVATION OF LINEAR RESONANCE FREQUENCY EQUATION.....56

APPENDIX E: MATLAB CODE.....59

E.1 Maximum Bubble Radius Function 59
F.2 Search Function 71
E.3 Finding Theoretical Size 72

REFERENCES ……74

LIST OF FIGURES

Figure 3.1a	Cavitation Difference	17
Figure 3.1b	Cavitation Difference	18
Figure 3.2	Optimal Seed 0.5 MHz	20
Figure 3.3	Optimal Seed 1 MHz	20
Figure 3.4	Optimal Seed 3 MHz	21
Figure 3.5	Optimal Seed 5 MHz	22
Figure 4.1	Bubble behavior results, 0.5 MHz	26
Figure 4.2	Bubble behavior results, 1 MHz	27
Figure 4.3	Bubble behavior results, 3 MHz	28
Figure 4.4	Bubble behavior results, 5 MHz	29
Figure 4.5	Pressure threshold	31
Figure 5.1	Experimental Apparatus	36
Figure 5.2	Experimental Apparatus	37
Figure 5.3	Surface Histotripsy	38
Figure 5.4	Internal Histotripsy	39
Figure 6.1	Smaller bubbles having more dramatic response	42
Figure 6.2	Frequency vs. pressure dependence	44

LIST OF TABLES

Table 3.1 Resonance size comparison 19

ACKNOWLEDGEMENT

First and foremost and I would to acknowledge Dr. Timothy Bigelow. Through his intelligence and hard work he was rewarded a much deserved career grant that has been able to fund my graduate experience. He has challenged me and stretched my brain to places I did not think possible, and done so in the kindest most patient fashion. I am forever grateful.

Special thanks to Charles Church (Associate Research Professor, University of Mississippi, Oxford, MS) for providing code that could be modified to calculate the bubble response. This work is supported by NSF grant Award ECCS-0643860 "CAREER: Ultrasound Histotripsy System Development to Improve Cancer Treatment."

I would also like to thank Dr. Scott McClure in Veterinary Clinical Sciences. He kindly provided tissue samples for this study on demand.

ABSTRACT

Medical ultrasound has shown great potential as a minimally invasive therapy technique. It can be used in areas such as histotripsy, thermal ablation, and administering medication. The success of these therapies is improved by the cavitation of microbubbles. This study evaluated the effect of varying the pressure amplitude on cavitation resonance frequency and the corresponding bubble size at therapeutic field levels. Other research indicated that the resonance size depends on pressure amplitude; however, that investigation only considered pressure amplitudes up to 1 MPa [MacDonald et al. (2004)]. Our study was conducted by simulating the response of air bubbles in water to linearly propagating sine waves using the Gilmore-Akulichev formulation to solve for the bubble response. The frequency of the sine wave varied from 0.5 to 5 MHz while the amplitude of the sine wave varied from 0.0001 to 5 MPa. The optimal seed size for a particular frequency of excitation and amplitude, which is normally only established for stable cavitation, was defined in our study as the initial bubble size that resulted in the maximum bubble expansion prior to bubble radius dropping below its initial radius. The simulations demonstrated a downshift in resonance size with increasing pressure amplitude. Therefore, at therapeutic levels, smaller bubbles can have a more dramatic response to ultrasound than larger bubbles.

CHAPTER ONE: OVERVIEW

The minds of engineers come in many varieties as can be seen in the complexity of subdivisions in each field. The beauty lies in the multitude of ways engineers can improve life for the current human race and those generations thereafter, including their capacity to further medical science. Second only to heart disease, cancer claims the most lives of United States men and women, with cancer related deaths climbing over half a million each year since 2006 [1]. In 2009 1.5 million Americans are projected to be diagnosed with cancer. The cancer cases affecting at least 25% of women and men are breast and prostate, respectively. A goal of engineers is to treat this disease by developing fortifying technology to make cancer treatment more accessible, successful, and less painful. Acoustic wave therapy can accomplish these goals, especially when targeted at the soft tissue.

The use of sound waves entered the medical community in the middle of the twentieth century. Most commonly it is used in obstetrics to view the development of the fetus. This is a diagnostic ultrasound example where the transducer is used to view the uterus during pregnancy. Diagnostic ultrasound has also been used for real-time imaging for guidance during surgical procedures. More recently the use of ultrasound has been accepted in therapeutic applications in addition to diagnostic applications. Minimally invasive procedures such as kidney stone treatment using a high intensity focused, know as shock wave therapy, ultrasound transducer and simple procedures such as heating joints and administering medications have been accepted by the Federal Drug Administration and are regularly employed. These procedures are generalized as therapeutic ultrasound. Kidney stones are broken up by using focused high-pressure sound waves; this process is termed lithotripsy. It is

safe, non-surgical, outpatient procedure because the acoustic shock waves are able to pass through the skin and soft tissue without significant damage. Physical therapists often use ultrasound as a treatment mechanism to stimulate blood flow in certain areas as well as using a topical medication and letting the acoustic waves carry it beyond the skin surface into the muscles and joints.

This research group, headed by principal investigator Dr. Timothy Bigelow, has been funded to explore advances in the field of high intensity focused ultrasound therapy, specifically, for cancer treatment of soft tissue organs. The research studies a new technique that has been developed using pulsed high intensity focused ultrasound, called histotripsy. Histotripsy's function can be identified in its root words. The Greek word 'histo' means body tissue and the word 'tripsy' translates into crush, grind, or break down. This procedure does breakdown unwanted body tissue into sub cellular structures by using microbubble cavitation induced in an ultrasonic field [2]. This process aims to destroy cells without damaging surrounding tissue similar to previously mentioned therapy procedures. Focused ultrasound energy passes through layers of skin, fat, muscles and overlaying soft tissue organs to reach its target without affecting those layers. The histotripsy research is motivated in part by thermal ablation, which is another focused ultrasound technique that uses heat to damage tissue cells. Histotripsy is an alternative to traditional, invasive surgery requiring scalpels and suctions and would reduce a patient's pain, cost, and recovery time if successfully developed and accepted by the medical community.

1.1 Background Therapeutic Ultrasound Work

For years ultrasound has shown remarkable potential as a tool for minimally invasive therapy. Recently, ultrasound thermal ablation of tissue has successfully treated some neoplasia and uterine fibroids [8]. The procedure uses the energy in the ultrasound waves to heat and kill targeted tissue and has been extensively studied [9, 10, 11]. In addition to killing the tissue, ultrasound therapies are being successfully developed to enhance thrombolysis [12], improve drug and gene delivery [13], control bleeding and hemorrhaging from severe trauma [11], erode or liquefy tissue [2, 3,14, 15] and destroy bacteria biofilms [16]. Many of these developing therapies have been found to depend upon or be significantly enhanced by the cavitation of microbubbles. Therefore, it is critical to understand the interaction of microbubbles with high intensity sound waves. Fully understanding the interaction will better ensure effective ultrasound therapy.

1.2 Background Histotripsy Work

High intensity focused ultrasound has been used in medicine to thermally ablate unwanted lesions. As with most medical procedures, there is risk involved and a goal should be to minimize the risk. Thermal ablation uses continuous ultrasound waves that can be focused to accurately locate and damage unwanted tissue with excessive heat. An approach using repetitive, very short pulses of high intensity controlled ultrasound has given promising preliminary results for tissue erosion [3]. The complex tissue and microbubble interaction in the focal region of the ultrasound beam gives rise to cavitation in the soft tissue region. The

intricate cavitation process produces mechanical damage resulting from extreme expansion and collapse of the oscillating microbubbles giving rise to microjets that shred the tissue into sub cellular fragments. Therapeutic tissue damage using histotripsy is largely based on the ability to induce, control, and manipulate microbubbles internally.

In the past decade new discoveries involving histotripsy research have been made. In this work the primary focus was targeted to perforate the left atrial septum of a newborn child diagnosed with hypoplastic left heart syndrome [4]. Either tissue removal via reconstructive surgery or a heart transplant is required for the neonates to live beyond two weeks after discovering this birth defect. Using ultrasound to erode the unwanted tissue was the goal of these studies. Porcine atrial wall samples submerged in a distilled, degassed water bath were exposed using a single element focused ultrasound transducer [3]. During these experiments many well defined holes were created in the tissue due to the cavitating microbubbles created by the high intensity ultrasound pulses. Since these initial histotripsy trials, varieties of the technique have been developed including transducer frequency, alignment, and pressure amplitudes of the acoustic wave [4]. More important than the multitudes of techniques that can be used to produce histotripsy is the actual desired effect, cavitation of microbubbles. The oscillating microbubble has complexities during the histotripsy process. If better understood, desired effects can be maximized to use ultrasound for surgeries including hypoplastic left heart syndrome and soft tissue neoplasia in the abdomen.

1.3 Background Cavitation Work

For hundreds of years scientists have noted interesting phenomena, referring to cavitation, but could not define it until the late 1800's due to the small order of magnitude at which the effects were occurring [5]. Cavitation is the expansion and collapse of a gas filled bubble in fluid. Acoustic cavitation is this same expansion and collapse of a gas bubble in fluid with the addition of an acoustic field. Previous research on bubble dynamics evolved from the equation of motion concerning the bubble, liquid and the pressure the system is under [6]. The equation of motion remains the building block for the complexity of the microbubble during the cavitation process.

The dependence of the frequency and the bubble size has always been a theoretical base for bubble formulations as well. This dependence can be derived from the equation of motion and has been used as a reference for many bubble formulations involving cavitation [7]. In previous works there has been some exploration of the bubble size relating to the frequency and pressure amplitude, seen in Flynn and Church [38]. In this work a dependency was shown relating both pressure amplitude and frequency for the normalized bubble size (maximum expansion to initial radius.) Flynn and Church show plots holding the pressure amplitude at a fixed state able to achieve cavitation (5 MPa) and vary the frequency from 0.1 to 10 MHz. As the frequency decreases the initial bubble size that gives the largest response increases. This result is expected by referencing the inverse relationship of bubble size and frequency [7, 21]. Their work then held the frequency constant and varied the pressure amplitude from 0.5 MPa to 5 MPa. These plots show that during the initial cycle the initial radius does not respond unstably until 2 MPa. These initial plots give a great reference for the

work completed in this work. The improvement was searching for a specific optimal seed size to achieve the greatest maximum collapse. Having these specific values for each frequency and pressure amplitude may lead to a better understanding of cavitation nuclei in biological tissue.

1.4 Research Objective

The ultimate goal of this research was to advance the use of histotripsy for soft tissue cancer treatment. Considering the background research and tools available, the general goal of the research was to develop a histotripsy system and to improve the system or procedure. The specific objective was to complete theoretical computations gaining knowledge to improve the excitation relationship between the oscillating microbubble and the undesired cancerous cells.

The quest for optimum damage to undesired cells via cavitation depends on many factors, some can be controlled and others cannot. The controllable factors would include the frequency of the therapy transducer, the size of the microbubble, and the pressure amplitude of the driving sound waves. The theoretical computations are aimed at optimizing the three controllable factors of the system, to achieve the most damage to the target tissues in the least amount of time. Given a range of frequencies the objective was to find corresponding bubble sizes at specific pressure amplitudes that would, in the future, optimize the physical system for histotripsy.

In this thesis, the response of a spherically symmetric air bubble in an unbounded water media to ultrasound waves was simulated. The goal was to determine how the

maximum bubble response depended on ultrasound frequency and bubble size for pressure amplitudes at therapeutic levels. The hypothesis was that as the pressure amplitude increased, the bubble size that resulted in the maximum response for a specific ultrasound frequency (i.e., optimal seed size) would decrease. Existing research shows a decrease in resonance size with increasing pressure [7], but that work only considered pressures less than 1 MPa, well below the acoustic pressures used to induce inertial cavitation in biomedical applications. These pressures have occurred up to 20 MPa. For the purposes of this study, the optimal seed size was defined as the initial bubble size that results in the greatest bubble expansion relative to the initial size prior to the bubble radius falling below the initial radius (i.e., first collapse).

1.5 Thesis Organization

This document contains the descriptive research procedure. Theoretical background research was completed; experiments were conducted using *ex vivo* tissue which corresponds to theoretical cavitation work; and mathematical models were shown using Matlab to further understand and improve the theoretical knowledge regarding microbubble response given preset input parameters. This thesis also contains an analysis of the simulation results and projected future work.

CHAPTER TWO: THEORY

2.1 Rectified Diffusion

In order for acoustic cavitation to occur, small gas bubbles must develop in a liquid. In general, a small gas bubble would likely diffuse into the surrounding liquid unless acted upon by an external force, such as an acoustic field. The sound field counteracts the normal process and at some threshold pressure will cause gas to diffuse into, instead of out of, the bubble. The increase of gas into the bubbles causes the bubble radius to grow in size; this process has been coined "rectified diffusion." [6] The rate of gas diffusion in a liquid is proportional to the concentration gradient of dissolved gas. As the bubble radius increases the concentration gradient also increases which causes an influx of gas molecules.

To mathematically explain the dynamics of a gas bubble in liquid the equation of motion is the building block. The Eq. 1 shown below refers to the motion of the bubble radius. It is assumed that the liquid properties are constant, the bubble remains spherical in shape, and that the acoustic wavelength is much larger than the diameter of the gas bubble.

$$\frac{d^2R}{dt^2} + \frac{3}{2R}\left(\quad\right) \quad \rho\left[\quad \sigma \quad \omega\right] \tag{1}$$

In Eq. 1, R represents the radius of the bubble, ρ is the density of the liquid, p_g is the pressure of the gas inside the bubble, σ is the surface tension, P_0 is the hydrostatic pressure in the liquid, and $P_A \sin(\omega t)$ is the driving force of the acoustic field. Flick's law of mass transfer is the equation used to demonstrate gas diffusion in and out of the bubble, shown in

Eq. 2. The concentration inside the gas bubble is assumed to be a constant; therefore, the diffusion refers to the surrounding liquid.

$$\frac{dc}{dt} = \frac{\partial}{\partial} \perp \mathbf{v}\bullet \tag{2}$$

In Eq. 2 c represents the concentration of the gas in the liquid, **v** is the velocity of the liquid and D is the diffusion constant. The diffusion equation and the equation of motion are dependent on one another through the velocity and change in concentration term in Eq. 2 as well as the p_g in Eq. 1. Epstein and Plesset [17] treated this problem by setting the gas bubble at rest in an infinite liquid; they found the rate of change for the number of gas moles in the bubble shown by Eq. 3. In Eq. 3, C_i is the initial uniform concentration of the gas (concentration at infinity) and c_s is the concentration of gas in the liquid at the bubble wall [17].

$$dn / dt = \quad - \quad + \tag{3}$$

If these formulations were to be useful to realistic processes, such as cavitation, a dynamic form must be solved. The derivation assumes that the bubble undergoes spherical and symmetrical motion only and there is negligible diffusion during a single oscillation of the gas bubble. The second assumption can be made due to diminutive diffusion occurring during an extremely fast oscillation. The general equation, developed by Eller and Flynn [6], for the flux of gas into the bubble can be seen in Eq. 4 where R_0 is the equilibrium radius.

$$\frac{dn}{dt} = \quad \left[\quad \left(\quad \right) \quad \right] \quad \left(\quad \right) \tag{4}$$

$$A = \frac{1}{T_b} \int_0^{T_b} \quad \tag{5}$$

$$B = \frac{1}{T_b} \int_0^{T_b} \quad \tag{6}$$

$$C_{sn} = \quad + \quad \tag{7}$$

In the above equations T_b is the period of the bubble, R is the radius of the bubble changing with time, and C_0 is the saturation concentration of the gas in liquid. The derivation of equations four through seven are seen in Appendix A.

To achieve rectified diffusion the pressure of the sound field must reach and exceed a certain pressure threshold. The threshold occurs at the moment the average diffusion is zero, and as the pressure is increased the concentration of gas in the bubble, C_i, also increases which causes the bubble to grow in size. For frequencies used in therapy procedures, the diffusion pressure threshold can be illustrated using the ratio of concentrations shown below:

$$\frac{C_i}{C_0} = \left[\quad \right] \tag{8}$$

The functions A and B depend on the bubble size over time found by using the equation of motion. The pressure threshold dependent variables end up being the pressure amplitude of

the incoming sound wave $P_{A,}$ the radius of the bubble, $R,$ and the frequency of the acoustic wave, ω.

2.2 Bubble Dynamics

Small bubble oscillations have been difficult to model. In order to obtain a direct formulation for bubble dynamics, assumptions had to be made. There have been three prominent models for small bubble oscillation; Rayleigh-Plesset, Keller-Herring, and the Gilmore model; two of which are directly correlated to the equations used for the mathematical computations in this thesis. The Rayleigh-Plesset model assumes the velocity of sound is infinite in liquid; the Herring model improves by assuming the velocity is a finite constant; and the Gilmore model allows the sound speed to vary depending on the specific liquid in which the bubble is oscillating [18]. These three formulations for a bubble oscillating in an acoustic field are all accredited, and used by many for different specialties in the field.

Rayleigh [19] was the pioneer in mathematically modeling the dynamic behavior of bubbles. Since his first published work in 1917, small improvements have been made on the original equation by Plesset [20] and Glimore [21]. The problem was solved for the collapse of a gas bubble in a significantly larger body of liquid. By ignoring the surface tension of the bubble and the viscosity the bubble boundary changing with time was solved by means of the momentum equation.

$$R\frac{d^2R}{dt^2} + \frac{3}{2}\left(\quad\right)^2 \qquad (9)$$

Eq. 9 shows change in radius as dependent on ρ, P_{∞}, and $P(R)$ which are the liquid density, pressure of the liquid at infinity, and the pressure of the liquid at the bubble boundary. Eq. 9 became the well-known Rayleigh-Plesset equation by simply adding the surface tension and viscosity effects as shown in Eq. 10.

$$R\frac{d^2R}{dt^2} + \frac{3}{2}\left(\quad\right)^2 \quad \left[\qquad\qquad \mu\left(\quad\right)\right] \qquad (10)$$

The derivation to the Rayleigh-Plesset equation using an energy balance approach is in Appendix B.

Gilmore [21] further improved this method. The Gilmore equation advances beyond the others by having capabilities for higher pressure fields. Additionally, it was presented in a form that could be computed to produce a large number of results in a reasonable amount of time. Gilmore [21] begins with the conservation of momentum regarding the vector velocity of a spherical bubble as it grows and collapses. A derivation of the Gilmore equation, shown in Eq. 11, is in Appendix C.

$$RU\frac{dU}{dR}\left(\quad\right) \quad \left(\quad\right) \quad \left(\quad\right) \quad \left(\quad\right) \qquad (11)$$

Although the Keller-Herrring equation is not used directly in the simulation computations, it is used to reference what the linear approximated resonant frequency would be at low pressure amplitudes. Eq. 12 is shown below in terms of pressure with β as an arbitrary parameter between $0<\beta<1$ and $P(t)$ the pressure in the liquid at the bubble wall.

$$\left[\quad \cdot \quad \cdot \quad \cdot \right. \\ \left| \quad \cdot\cdot \quad \cdot \quad \right| \\ \left[\quad \right] \quad \left[\quad \right] \quad \left[\quad \right] \quad \left[\quad \right] \qquad (12)$$

2.3 Cavitation

Cavitation is the response of gas bubbles in liquid after oscillating to an acoustic field. There are two specific types; stable and inertial cavitation. Stable cavitation is the relatively small oscillations of the bubble's radius about its equilibrium radius. These oscillations may generate microstreaming in the vicinity of the bubble leading to improved sonoporation, but otherwise have little effect on the tissue. The amplitude of the oscillations during stable cavitation experiences a resonance that depends on the size of the bubble and frequency of the sound. When a bubble is driven at its resonant frequency it reaches higher oscillation amplitudes and will provide more effective therapy. The resonance frequency for a particular bubble size also depends on the ambient pressure, surface tension, and the liquid density. When measuring the resonance response during stable cavitation, numerous acoustic cycles are often needed to allow the transient behavior of the dynamic system to fade.

Inertial cavitation is the dramatic expansion and violent collapse of the gas bubble that occurs at higher acoustic pressure levels. During inertial cavitation the bubble expands to many times its original size and collapses violently causing microjets that can shred tissue. Inertial cavitation occurs over a small number of acoustic cycles, usually three or less, before the collapse takes place. Therefore, it is more difficult to determine the resonance size/frequency for a bubble undergoing inertial cavitation because numerous acoustic cycles cannot be used to remove the impact of other transients in the dynamic system.

CHAPTER THREE: SIMULATIONS

This chapter will discuss the reason for simulating bubble behavior in an ultrasound field, programming code, mathematics used, and the justification for a new definition of optimal seed size.

3.1 Simulation Motivation and Code

To better understand bubble activity the numerical computing system, MATLAB was used. To have an idea about what is happening to a bubble on the micron order of magnitude a computing system was necessary. The original code was written in Fortran by Dr. Charles Church. After the code was converted to be read using the MATLAB system other modifications were made. The code was written to calculate the response of bubbles to a sine wave. The phase of the acoustic pressure in the programming code was initially set to be negative; in order to compensate for this a negative pressure value was entered to achieve reasonable results. The modified code had nineteen initial inputs that remained constant throughout each simulation. These constants were defined as P(2) through P(20) and are in Appendix E section C.1 with the rest of the attached code.

As can be seen in the list of constants, the simulations involved a single air bubble in water. The variables were pressure amplitude and frequency The search function, shown in Appendix C part C.2, was written to scan initial bubble sizes searching for the maximum expansion relative to the initial size, prior to when the bubble dropped below its initial size.

Finding this optimal seed size was the primary goal of the simulations. Our optimal seed size was also used to find the maximum bubble expansion relative to the initial size over 50 acoustic cycles or until the initial radius dropped below one tenth its initial size (neglecting bubble fragmentation and assuming rebound). The simulations found the optimal seed size for pressure amplitudes of 100 Pa to 5 MPa for acoustic frequencies of 1, 3, and 5 MHz. These pressures and frequencies were selected based on their relevance to therapeutic ultrasound.

3.2 New Definition of Optimal Seed Size

The traditional definition of resonance size stems from a relationship between the frequency of the acoustic waves and the bubble radius in the acoustic field. A bubble at the resonance size for a particular frequency would undergo maximum changes to its radius when excited at that frequency once any transient behavior of the dynamic system has subsided. The oscillations for bubbles of a different size would be less than the oscillations at the resonance size. The relationship between resonance frequency and resonance size for low level acoustic excitations is given by the following equation:

$$f_0^{lin} = \frac{1}{2\pi} \sqrt{\frac{2\Gamma}{\rho}\left(\right)} \tag{13}$$

In Eq. 12 Γ is the polytropic exponent of the encapsulated gas in the microbubble and R_o is the initial bubble radius [7] . A derivation for this is in Appendix D starting with Eq. 11, the Keller-Herring equation of bubble dynamics.

While this traditional definition of resonance size works well for stable cavitation applications, resonance size is impossible to define when inertial cavitation is present. When undergoing inertial cavitation a single bubble would typically undergo one expansion prior to a violent collapse, which would leave the bubble in fragments. Furthermore, even if the bubble did not fragment and the bubble radius rebounded for many cycles, the bubble's response would not be periodic as is illustrated in Figure 3.1. Figure 3.1(a) shows a bubble undergoing stable cavitation while Figure 3.1(b) shows a bubble undergoing inertial cavitation and rebound as simulated in our study. The transient behavior in Figure 3.1(a) passes after about 5 to 10 acoustic cycles, leaving a periodic sinusoidal oscillation while the oscillations in Figure 3.1(b) never exhibit any periodicity even out to 50 acoustic cycles. Therefore, it is impossible to "wait" until the transient behavior of the system has subsided when determining a resonance size/frequency for a bubble undergoing inertial cavitation. For this reason, a modified definition of resonance size was used in our study.

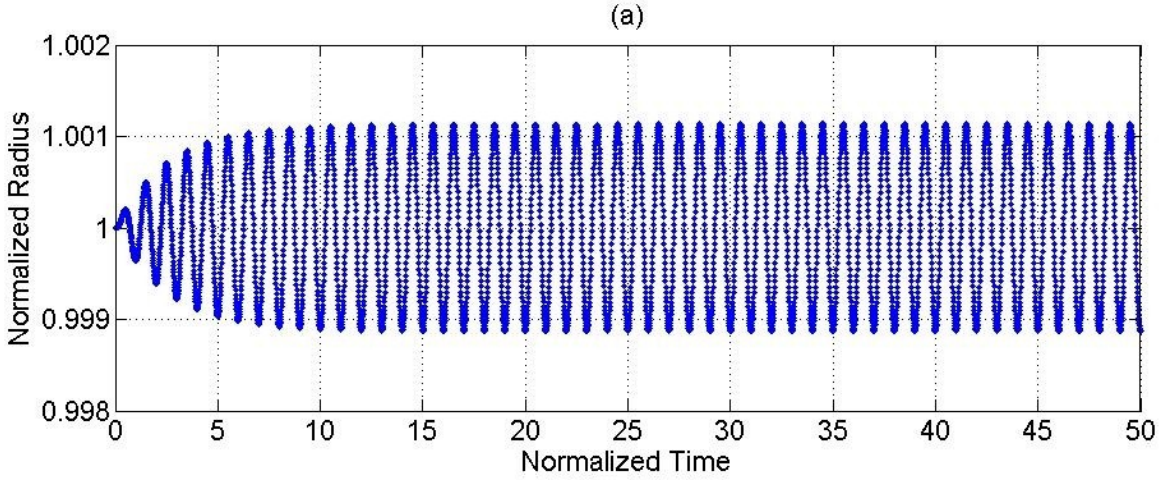

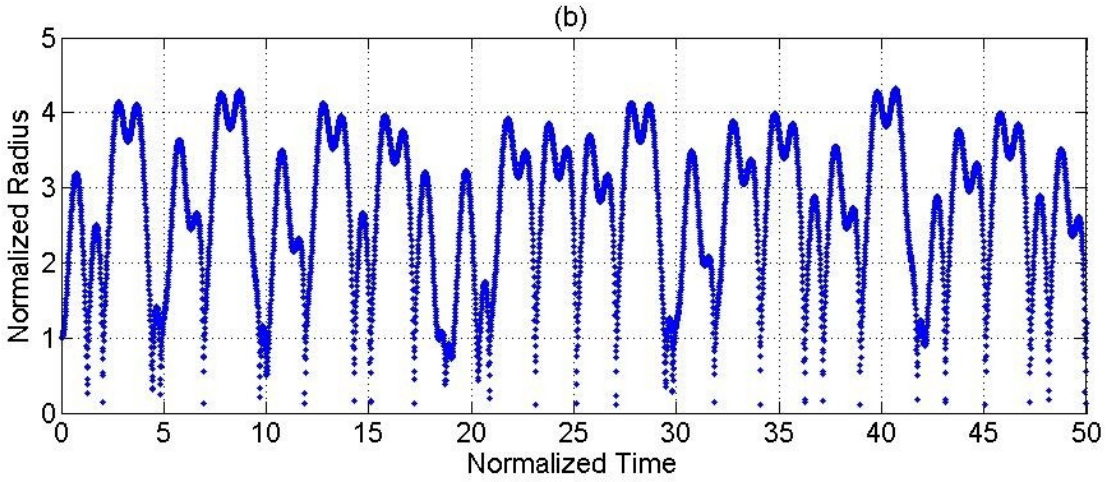

Figure 3.1: A bubble undergoing stable cavitation is shown in part (a). The simulated bubble was driven at 1 MHz and 1 kPa. The bubble oscillation shown in (b) was driven at the same frequency, 1 MHz but with a higher pressure amplitude, 1 MPa. Both plots show the radius normalized to the initial radius.

When determining a resonance response for inertial cavitation, we defined the optimal seed size for a particular acoustic frequency as the initial bubble size that resulted in the largest bubble expansion prior to when the size of the bubble dropped below its initial size (i.e., first collapse). This definition avoids the complication of bubble fragmentation that would alter the bubble size while still providing some guidance to inertial cavitation based therapies. For consistency, this definition was used throughout the entire range of pressure amplitudes rather than just for amplitudes where inertial cavitation was expected. Our new definition for optimal seed size does not generally give the same size as the traditional definition even for smaller excitation pressures inducing stable bubble oscillations as is illustrated in Table 3.1.

Frequency	0.5 MHz	1 MHz	3 MHz	5 MHz
Traditional/Theoretical Resonance Radius	7.01 μm	3.704 μm	1.4316 μm	0.946 μm
New Optimal Seed Radius found in Simulations	5.203 μm	2.993 μm	1.422 μm	0.941 μm

Table 3.1: Comparisons between the traditional definition of resonance size and our new definition of optimal seed size developed to study the relationship between bubble size and frequency at higher pressure amplitudes.

Table 3.1 shows both the traditional/theoretical resonance size and the new optimal seed size found under our new definition. The traditional size was found from Eq. 11 while the new size was found via computer simulations for a pressure amplitude of 100 Pa. The new optimal seed size is approximately the same as the traditional size for 3 and 5 MHz, but differs significantly at the lower frequencies. This difference can be attributed to variations in the transient behavior of the microbubble system as is illustrated in Figures, 3.2-3.5.

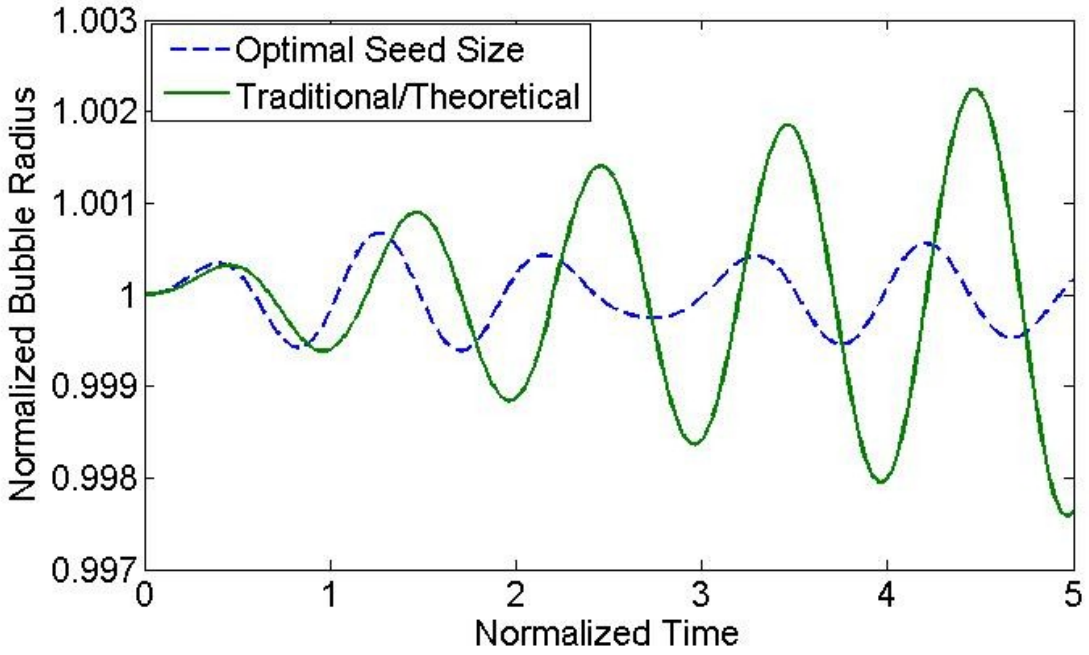

Figure 3.2: The normalized radius (radius/initial radius) versus normalized time (time/period of acoustic wave) when the initial radius is our new optimal seed size (dashed line) and the theoretical/traditional resonance size (solid line) for a 100 Pa, 0.5 MHz acoustical excitation of the bubble.

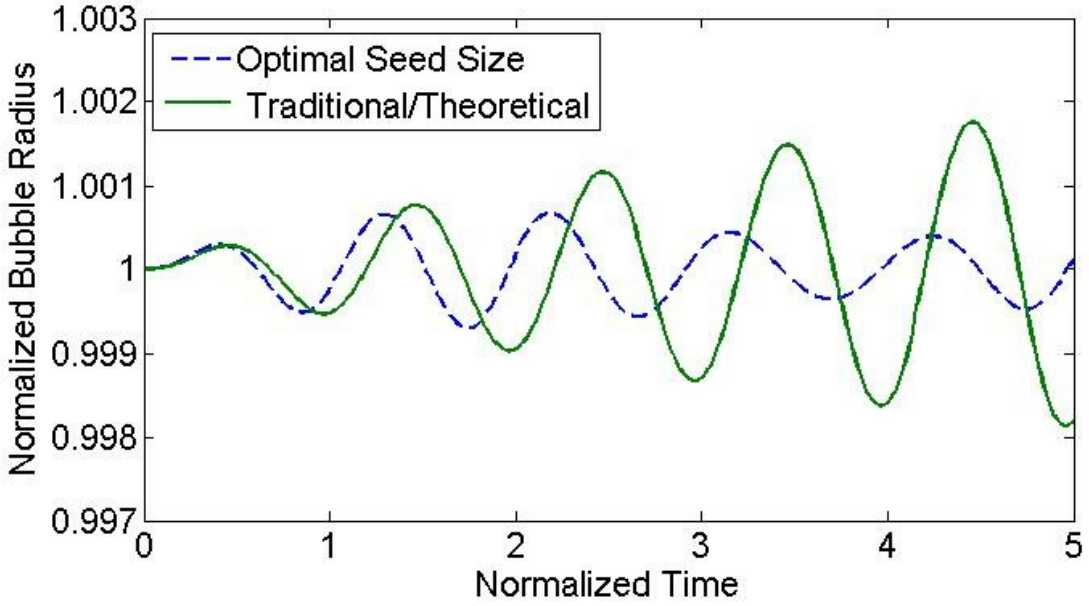

Figure 3.3: The normalized radius (radius/initial radius) versus normalized time (time/period of acoustic wave) when the initial radius is our new optimal seed size (dashed line) and the

theoretical/traditional resonance size (solid line) for a 100 Pa, 1MHz acoustical excitation of the bubble.

Figures 3.2 and 3.3 for the 0.5 MHz and 1 MHz cases, show within the initial cycle that the simulated optimal seed size has a slightly larger peak value than the theoretical resonance size. After the transients subside, however, the peaks level out smaller than the theoretical resonance peaks. The theoretical cycles continue to increase until reaching steady state with peaks approximately five times greater than the new optimal seed sizes. In Figures 3.4 and 3.5, however, which corresponds to the 3 and 5 MHz cases, the initial transient behavior of the theoretical and new optimal seed sizes are nearly identical.

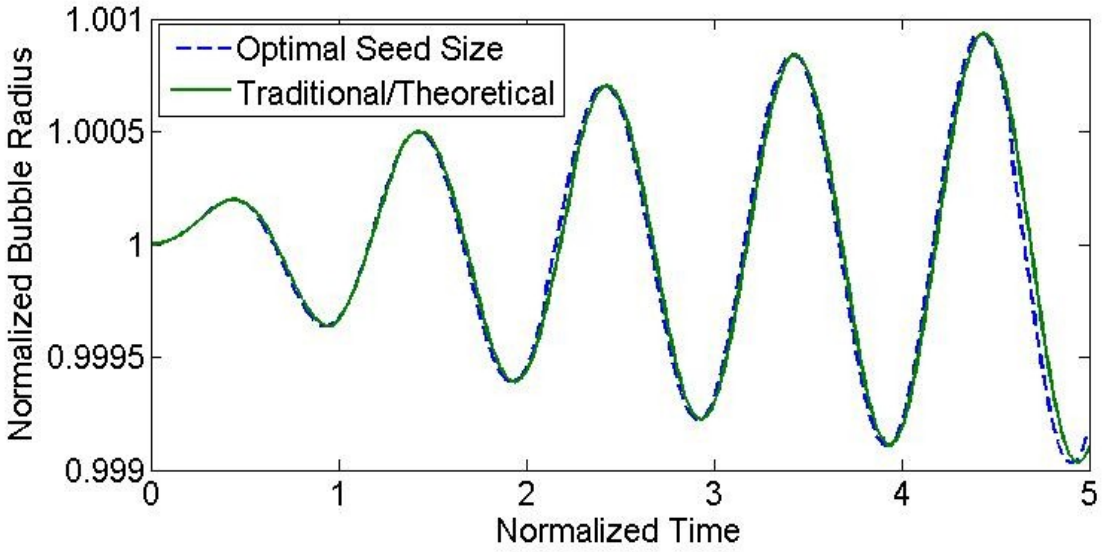

Figure 3.4: The normalized radius (radius/initial radius) versus normalized time (time/period of acoustic wave) when the initial radius is our new optimal seed size (dashed line) and the theoretical/traditional resonance size (solid line) for a 100 Pa, 3 MHz acoustical excitation of the bubble.

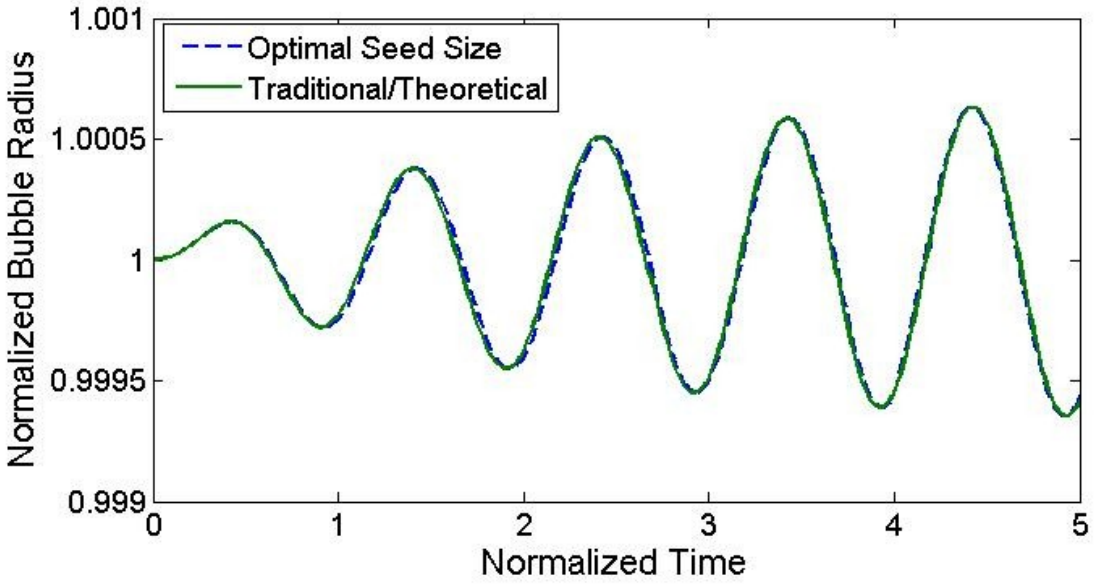

Figure 3.5: The normalized radius (radius/initial radius) versus normalized time (time/period of acoustic wave) when the initial radius is our new optimal seed size (dashed line) and the theoretical/traditional resonance size (solid line) for a 100 Pa, 5 MHz acoustical excitation of the bubble.

3.3 Equations Solved

The response of the bubbles to the acoustic wave was simulated by solving the Gilmore-Akulichev formulation for bubble dynamics [22, 23], which is given by,

$$R\left(\quad\right)\quad\left(\quad\right)\quad\left(\quad\right)\quad\left(\quad\right)\quad\left(\quad\right) \tag{14}$$

Eq. 13 represents the response of a single bubble with respect to time. The R corresponds to the radius of the bubble and U is the bubble wall velocity (i.e., $U =$). The other parameters in Eq. 12 are given by,

$$C = \lfloor \qquad \rfloor^{1/} \tag{15}$$

$$H = \int_{P\infty}^{P(R)} \frac{dP}{\rho} \tag{16}$$

In these equations, C is the speed of sound at the bubble wall and is calculated from the infinitesimal speed of sound in the liquid, C_o, a constant m normally set to 7, and the enthalpy of the liquid, H. The enthalpy is related to the pressure in the fluid far from the bubble, P_∞, and the pressure at the bubble wall, P(R). These pressures are given by:

$$P_\infty = \quad - \quad \tag{17}$$

$$P(R) = \quad - \frac{2\sigma}{R} - \left(\quad \mu \quad \right) \tag{18}$$

Here P_o is the ambient pressure of the liquid, $p_{acoustic}$ is the pressure associated with the acoustic wave, P_g is the pressure of the gas inside the bubble, σ is the surface tension of the bubble wall, and μ is the coefficient of shear viscosity. In addition, the time varying pressure is related to the time varying density of the liquid, ρ, represented by

$$P = \qquad\qquad - \tag{19}$$

Here ρ_o is the equilibrium liquid density of the fluid while α and β are constants describing the fluid.

The Gilmore-Akulichev formulation was selected for the study because it is capable of calculating the response of a bubble at higher acoustic pressures (prior to bubble fragmentation) without requiring the complexity and computational cost of three dimensional

models of bubble dynamics. Other models such as Rayleigh-Plesset or Keller-Herring, while popular with simulating bubble dynamics for contrast agent and some drug delivery studies [7, 24, 25, 26, 27], are not valid when the bubble expands more than several times its initial radius [28]. In addition, three-dimensional models are not required since the bubble is oscillating in isolation in an unbounded fluid (symmetric collapse), and the research was only interested in bubble behavior prior to the inertial collapse when bubble fragmentation is likely. The problem was further simplified by assuming that the ultrasound waves were not corrupted by nonlinear propagation distortion so that the acoustic excitation only had a single frequency (i.e., no harmonics or sub-harmonics).

CHAPTER FOUR: SIMULATION RESULTS

4.1: DEPENDENCE ON OPTIMAL SEED SIZE

The dependence of optimal seed size as a function of pressure amplitude is shown in Figures 4.1-4.4. It is clear from these Figures that with increasing pressure amplitude there will be a reduction in the resonance bubble size. They also show the maximum expansion relative to the initial size when the simulations are allowed to continue over 50 cycles or until the initial size dropped below one tenth its initial size. The maximum expansion of the bubbles also appears to increase dramatically as the optimal seed size of the bubble decreases. Therefore, the drop in optimal seed size probably correlates with the onset of inertial cavitation.

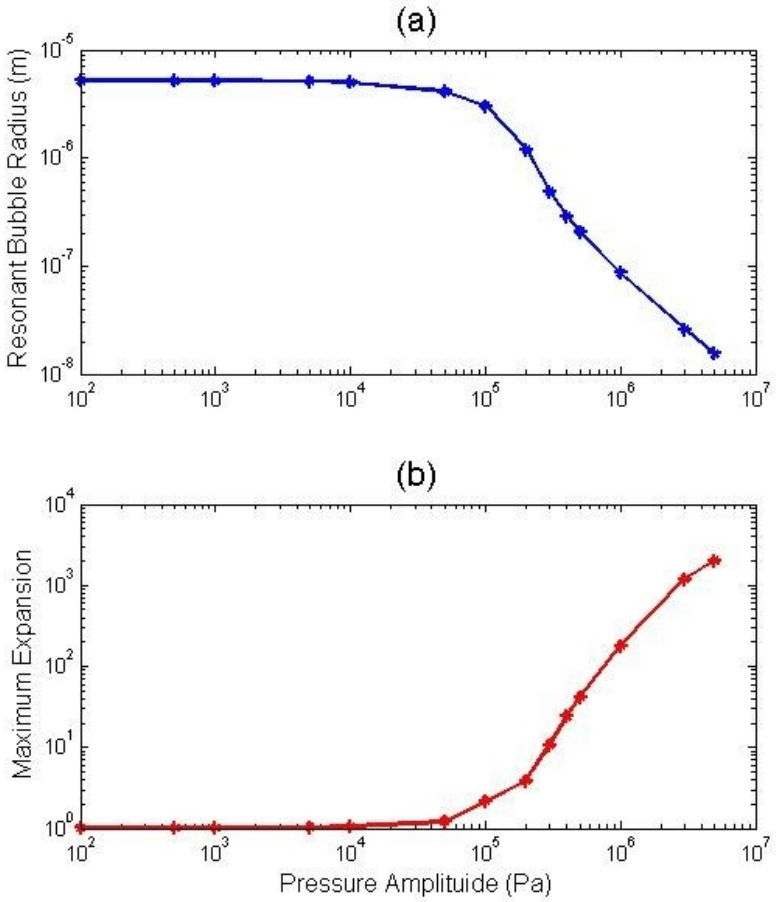

Figure 4.1: The plots correspond to 0.5 MHz frequency. The top graph (a) represents a decrease in bubble size as the pressure increases and the bottom graph (b) corresponds to the maximum expansion relative to initial size.

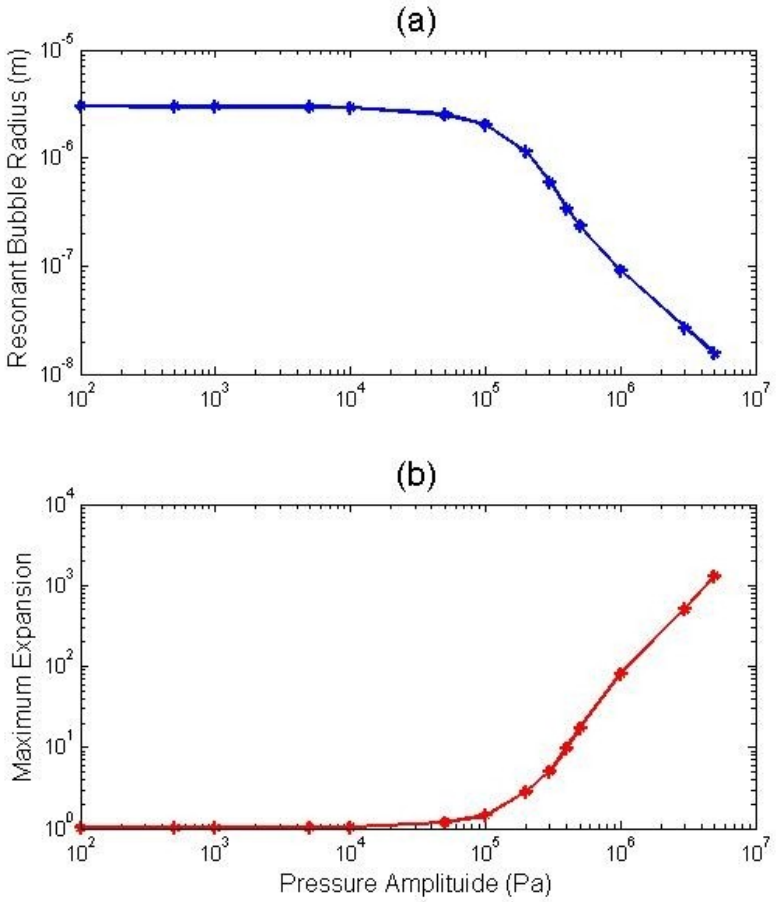

Figure 4.2: The plots correspond to 1 MHz frequency. The top graph (a) represents a decrease in bubble size as the pressure increases and the bottom graph (b) corresponds to the maximum expansion relative to initial size.

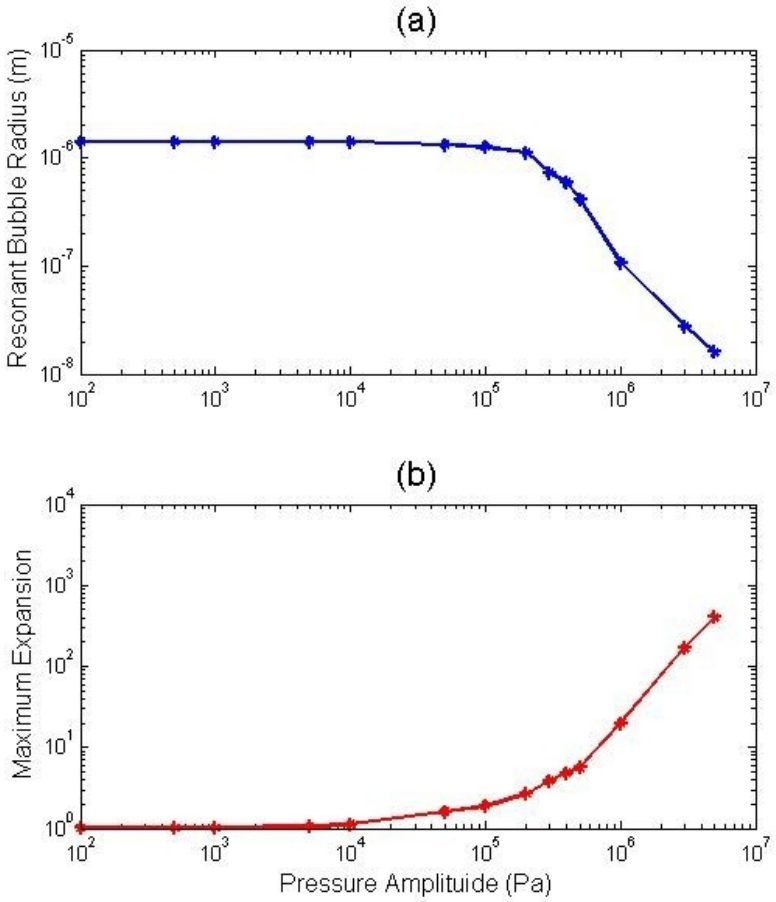

Figure 4.3: The plots correspond to 3 MHz frequency. The top graph (a) represents a decrease in bubble size as the pressure increases and the bottom graph (b) corresponds to the maximum expansion relative to initial size.

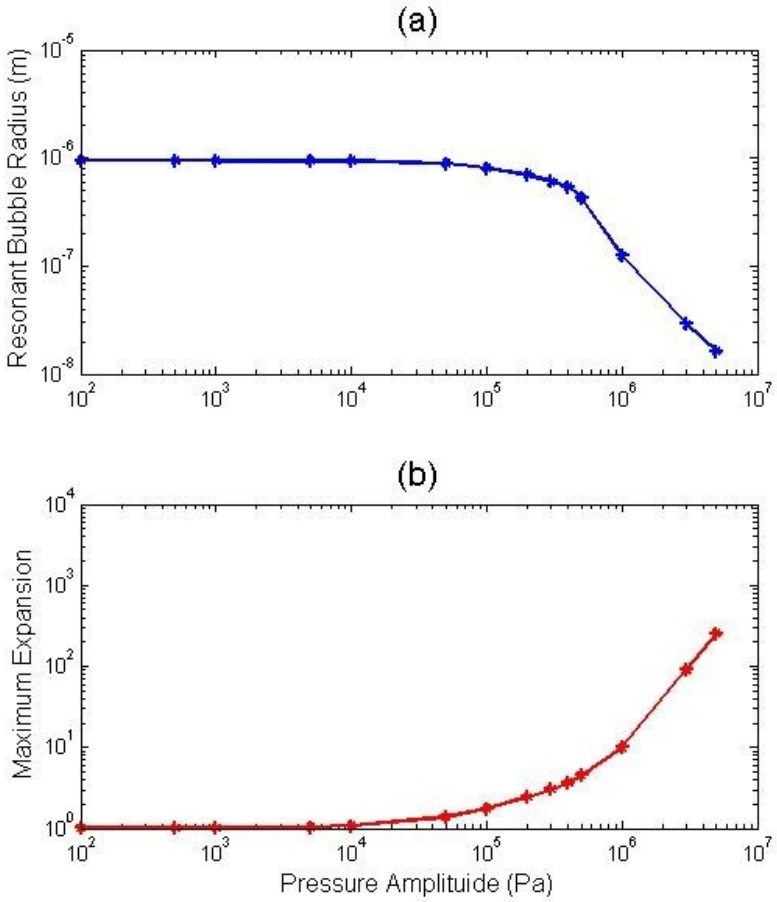

Figure 4.4: The plots correspond to 5 MHz frequency. The top graph (a) represents a decrease in bubble size as the pressure increases and the bottom graph (b) corresponds to the maximum expansion relative to initial size.

4.2: Pressure Threshold

To better understand these results, the pressure threshold corresponding to the dramatic drop in optimal seed size and the dramatic increase in expansion were determined for each frequency. The threshold values were determined by first fitting lines to the last three points in each plot for optimal seed size and also for the maximum expansion. These four points corresponded to pressure amplitudes of 0.5, 1, 3, and 5 MPa. The pressure threshold was then given as the pressure amplitude where this line intercepted the optimal seed size (dashed line) and the expansion sizes (solid line) at low excitation levels (i.e., 100 Pa) The pressure threshold values for all four frequencies for both resonance size and expansion are shown in Figure 4.5.

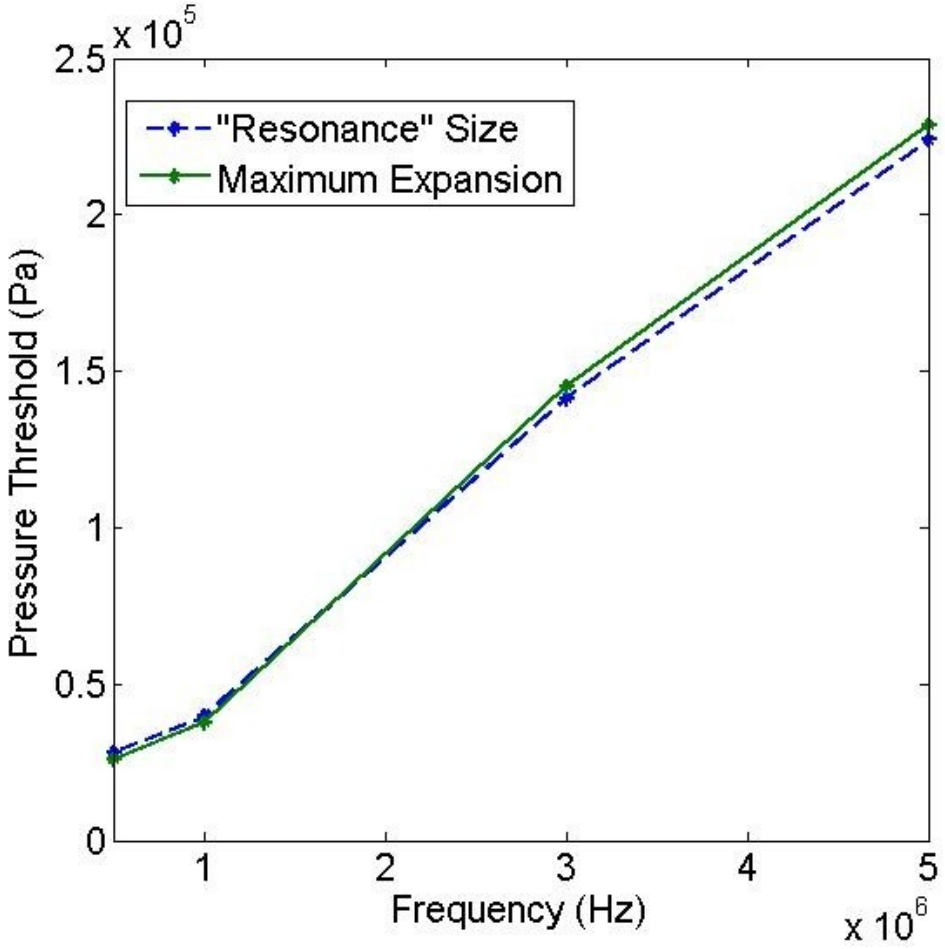

Figure 4.5: The pressure threshold in Pascals for frequencies of 0.5 through 5 MHz for both the dramatic reduction in optimal seed size and the dramatic increase in maximum expansion.

The pressure threshold corresponding to the dramatic drop in optimal seed size with pressure increases linearly with frequency, similar to what has been observed for inertial cavitation thresholds in other research [29]. Also, the threshold for the dramatic drop in resonance size is the same as the threshold for the dramatic increase in expansion indicating both effects have the same cause.

CHAPTER FIVE: EXPERIMENTS USING *Ex Vivo* PORCINE LIVER

To parallel the theoretical work and potential clinical application my work involved handling and performing experiments using *ex vivo* bovine and porcine liver. This section will discuss how the tissue was prepared, the workings of the experimental set-up used, and the results of the completed experiments.

5.1 Tissue Preparation

Choosing a soft abdominal tissue was done to make the transition from *ex vivo* to *in vivo* easier. As sound travels through various media it is more difficult to control the properties of the acoustic wave, leading to the possibility that those properties may change once they reach the target. Attenuation, absorption, and scattering will all occur when the sound source crosses the various barriers of the body. Parenchymatous abdominal organs have fewer acoustic interfaces making it a good starting point for ultrasound therapy. Using a soft tissue organ *ex vivo* would increase the likelihood of successfully repeating the experiment *in vivo*.

Both bovine and porcine liver were tested in the system. Initially bovine was used. Due to the size of a single liver it was challenging to dismantle the organ into pieces suitable for the experiment that sought to simulate the size and properties of a human liver. Also, the time between which the liver was removed from the animal and used in the experiment was a critical factor. The longer the organ is *ex vivo* the less realistic it becomes and the less useful the tests results then would be. A transition to porcine liver was made that improved all aspects of tissue preparation. The porcine provided a smaller liver and one that had more

characteristics to human tissue. Normal porcine liver contains five usable lobes. One lobe is a suitable size for an experiment that can be prepared simply by cutting a lobe from the organ and cleaning it under running water for at least five minutes to prevent excess blood in the experimental system.

In initial trials the tissue sample was placed in a small vacuum sealed plastic wrap prior to use. The plastic, though thin, was later revealed to have a negative effect of the alignment process of the source as well as possibly interfering with the therapy. The vacuum sealed plastic was discarded and the tissue went straight from cleaning into the experimental apparatus. This step did improve the accuracy of the alignment as well as results. The final tissue preparation improvement was to place the clean single lobe into a cylindrical gas chamber submerged in distilled water. The degassing of the tissue removed air bubbles accrued during exposure time between the harvesting, packaging and cleaning. This removal of air bubbles drastically improved results during the experiments. This also correlates to *in vivo* cases much more than tissue with accumulated gaseous bubbles. In the human body gas bubbles do not occur naturally.

5.2 Experimental Apparatus

Apparatus for the *ex vivo* tissue experiments consisted of a waveform generator, an amplifier, a matching network, and a single ultrasound transducer. To locate objects using the transducers a pulse echo was sent into the matching network and the reflections were monitored by an oscilloscope. The transducer is operated by a precise, three dimensional

motion system controlled manually or by a computer. The transducer is submerged into a water bath placed below the controlled motion system. The water bath fills a 20x20x10 plexiglas tank. The tissue sample is placed on the floor of this tank to be treated by the system.

The waveform generation can be an arbitrary sine wave, but the setting cannot, in this specific set-up. Two types of waveform generators were used to treat the tissue samples in these experiments: a computer card and an arbitrary generator by Agilent 33220A. The Agilent generator does not depend on the reliability of the computer or the program that controls it, LabView. These factors make using a arbitrary generator a more reliable choice. To achieve the tissue damage by histotripsy the generator was set to emit a sine wave with eight hundred and fifty volts peak-to-peak. This was the voltage limitation due to the power amplifier. The period cycle was five milliseconds, a twenty second pulse with a duty cycle of 3.6%.

The amplifier used was made by E&I Ltd., model number 1140LA-CI. It is a broadband solid state amplifier covering the frequency range of 100 KHz to 3MHz. Over 1500 Watts can be produced and it has a 55 dB gain. The main limitation with this amplifier is that its input voltage must be 1.0 Volts RMS to ensure no damage will be done to the amplifier.

The output of the amplifier is connected to the matching network and then the ultrasound transducer. The matching network was manufactured specifically for each 1.1 MHz ultrasound source. The sources are focused and concave used singly. Transducers 58 and 59 are used with no preference or limitations to either one. The focal lengths were tested in

the water bath using a single wire. The difference between the two transducers were slight, but found in the focal lengths. Transducer 58 had a focal length of approximately 64.064 mm and Transducer 59 focused at 64.351mm.

To locate the reflections a Panametics pulser module model number 5900 was used. It sends in a pulse/echo using a 200 Hz PRF, 32 J of energy, with the sampling at 50 Ohms, a high pass filter of 1 MHz and a low pass filter of 50 MHz. The attenuation was set to 35.5 dB and the gain was 40 dB. These settings gave a clear signal of the pulse and the echoes off the different surfaces, such as the top of the tissue, bottom of tissue and the plexiglas tank. Using these echoes as well as the knowledge of the transducer focal lengths, the focus can be set to wherever the desired region inside the tissue sample. After the source has been aligned using the pulse/echo method the connections were reattached and the wave generator sent the sine wave into the amplifier which reached the sample through the transducer. To monitor the area treated by the system the three dimension motion controller holding the transducer was given a preset grid to scan. The settings were input in LabView. These settings are up to the controller's discretion depending of the area to be treated. The time spend on each spot can also be controlled. The longer the step pause the more probable damage to the tissue at that particular point. In the experiments performed the step pause was always set to one minute. The experimental set up can be seen in Figure 5.1, and Figure 5.2 shows an enlarged view of the transducer and tissue.

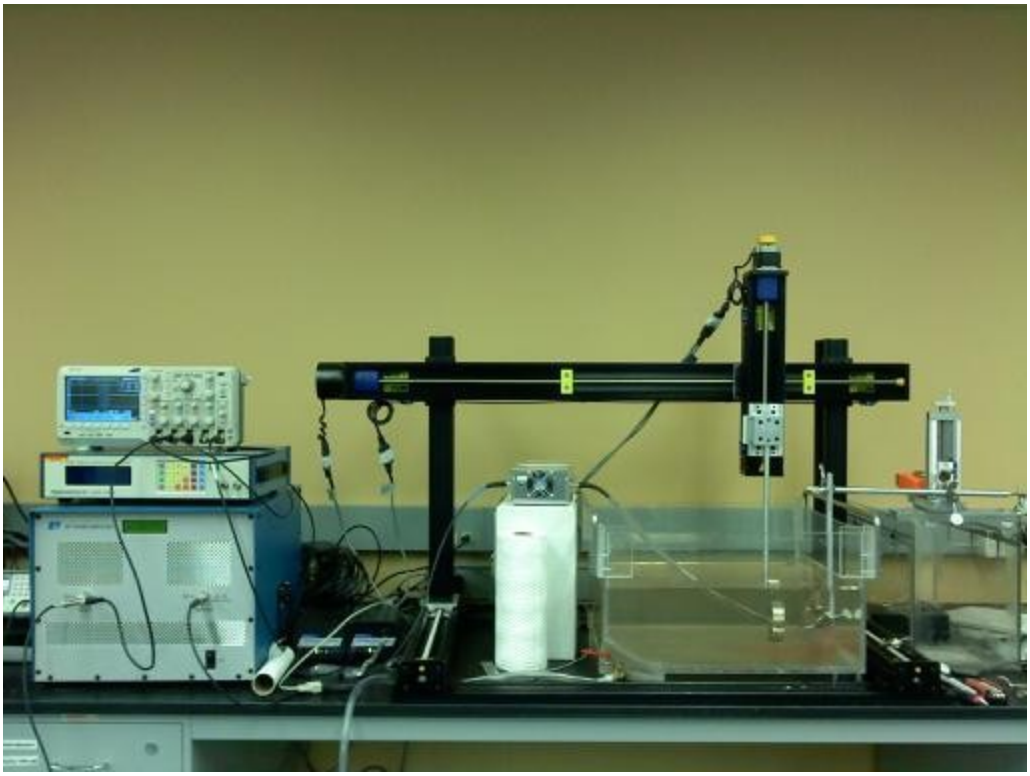

Figure 5.1: Pictured is the three dimensional axis holding the transducer, which is facing the liver tissue. The transducer cord is attached to a matching network that receives the amplified wave from the RF amplifier.

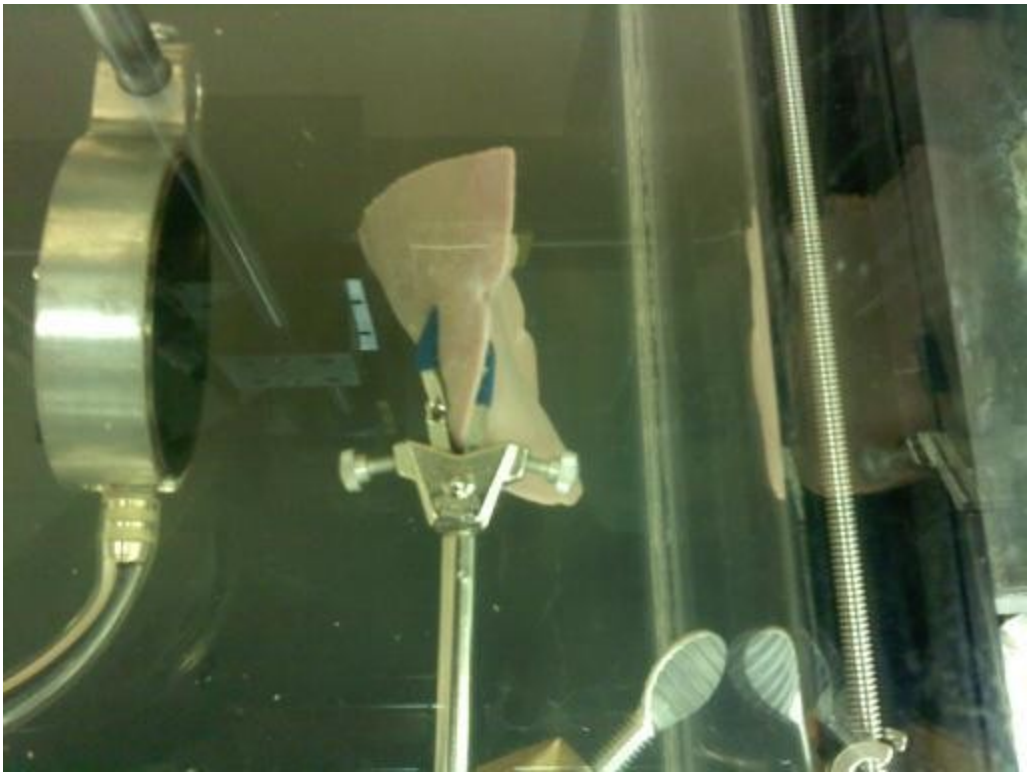

Figure 5.2: This photo shows the view from the top of the water bath. The three prong holder grips the tissue as the high pressure amplitude sound wave works on dissipating a well in the middle.

5.3 Experimental Results

The results depended greatly on the equipment used and how the tissue had been prepared. When the E&I amplifier was purchased the source was given enough voltage to destroy the tissue. Prior to this amplifier being employed, some discolorations were seen, but there was no dissipation of tissue; therefore, no histotripsy was occurring. The likely outcome was some light thermal ablation. Secondly, degassing the porcine tissue sample also greatly increased the results of the experiment that is histotripsy could be seen in the tissue with the naked eye. The damage looked like multi pinpoint foci. In the first case, shown in Figure F.3, the damage done is significant but not as applicable because the water bath used was not

degassed water. This caused the bubble interaction on the top of the tissue to create a trench. Although exciting, the parameters are not realistic for a typical situation considering bubbles do not occur naturally in humans. Figure three shows another trench inside the tissue sample. This achievement was much more encouraging because the parameters were ideal and the damage was done inside the sample, which would be applicable to a real life scenario.

Figure 5.3: Histotripsy seen atop the tissue sample.

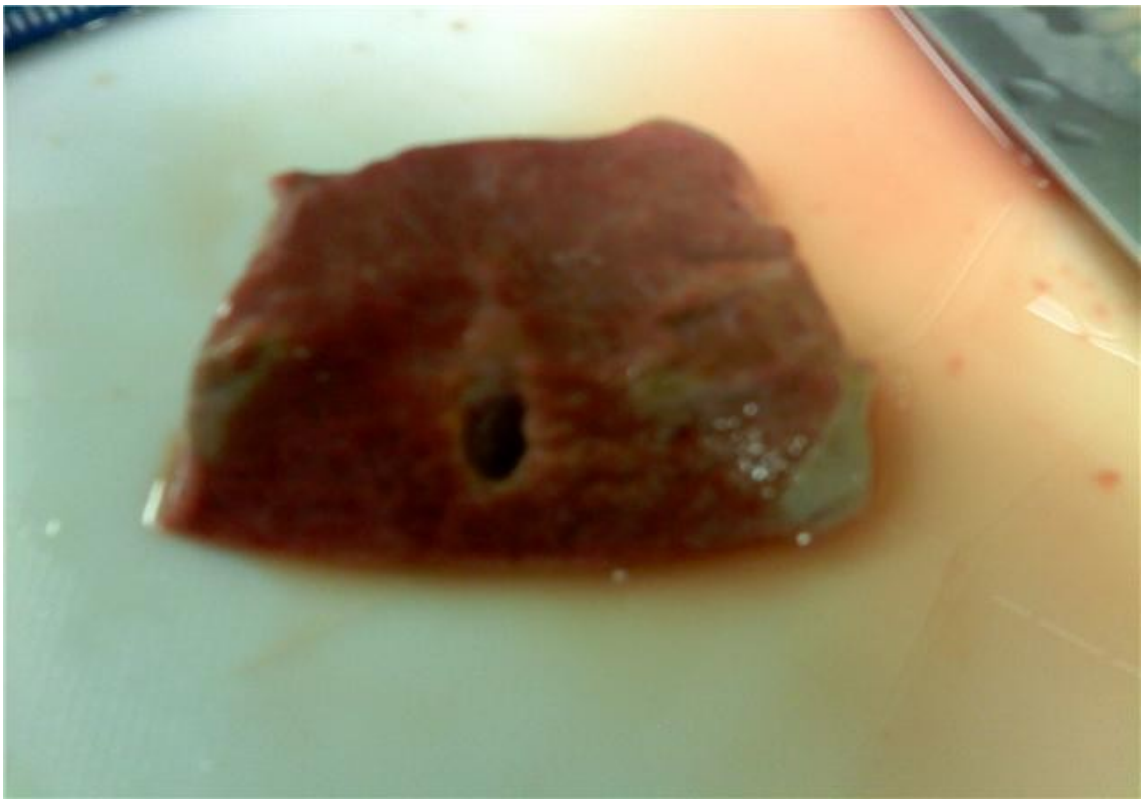

Figure 5.4: Histotripsy seen inside the tissue sample after layers were sliced off the top.

Future experiments to refine the study more precisely adjust the treatment settings and use a diagnostic transducer to view bubble cloud activity during treatment.

CHAPTER SIX: DISCUSSION

In my research, a single, spherical air bubble in water was simulated mimicking the response it would have in an ultrasonic field. The bubble displayed oscillations when driven at therapeutic pressure levels. Given the ultrasound frequency and bubble size, the goal was to establish how the maximum bubble response was dependent on these parameters. It was proposed that the optimal seed size of the bubble for any given ultrasound frequency would decrease as the pressure amplitude increased. The optimal seed size was defined as the bubble size that resulted in the largest expansion prior to the bubble radius decreasing to below its original size, which occurred in one cycle. Using this definition, the optimal seed size was used to simulate bubble responses over fifty cycles or until the bubble drops below one tenth its initial size and the maximum expansion relative to the initial size was found. Results have shown that as the pressure amplitude increases beyond some threshold, the optimal seed size of the bubble decreases, confirming our hypothesis. In addition, the maximum expansion of the bubble dramatically increases at the same threshold pressure. This pressure threshold is linearly dependent on frequency and is probably due to the onset of inertial cavitation that has been shown to increase linearly with frequency [29].

Considering the simulations demonstrated a downshift in resonance size with increasing pressure amplitude, the hypothesis was made that smaller bubbles can have a more dramatic response to therapeutic ultrasound than larger bubbles. To further explore this possibility, the initial bubble size was varied about the optimal seed size found previously, and the maximum expansion relative to the initial size was determined for a 1 MHz 100 Pa

(Figure 6.1(a)) and for a 5 MPa (Figure 6.1(b)) sinusoidal excitation. The peak shown in Figure 6.1(a) corresponds to the theoretical resonance size while the peak in Figure 6.1(b) corresponds to the optimal seed size that the search function revealed. These scaled input values support that smaller bubbles would have a more dramatic effect in therapeutic applications. The plots also show that as the pressure amplitude increases for the system the resonance peaks change shape. In the lower pressure amplitude case shown in Figure 5.1(a) the resonance peak is narrow while in the high pressure amplitude case the optimal seed peak is much broader. This indicates that at higher pressure levels it is less critical to use bubbles at resonance size to achieve results. The resonance peak at higher amplitudes is also asymmetric indicating that the bubbles less than optimal seed size will not respond independent of the pressure amplitude of the acoustic wave.

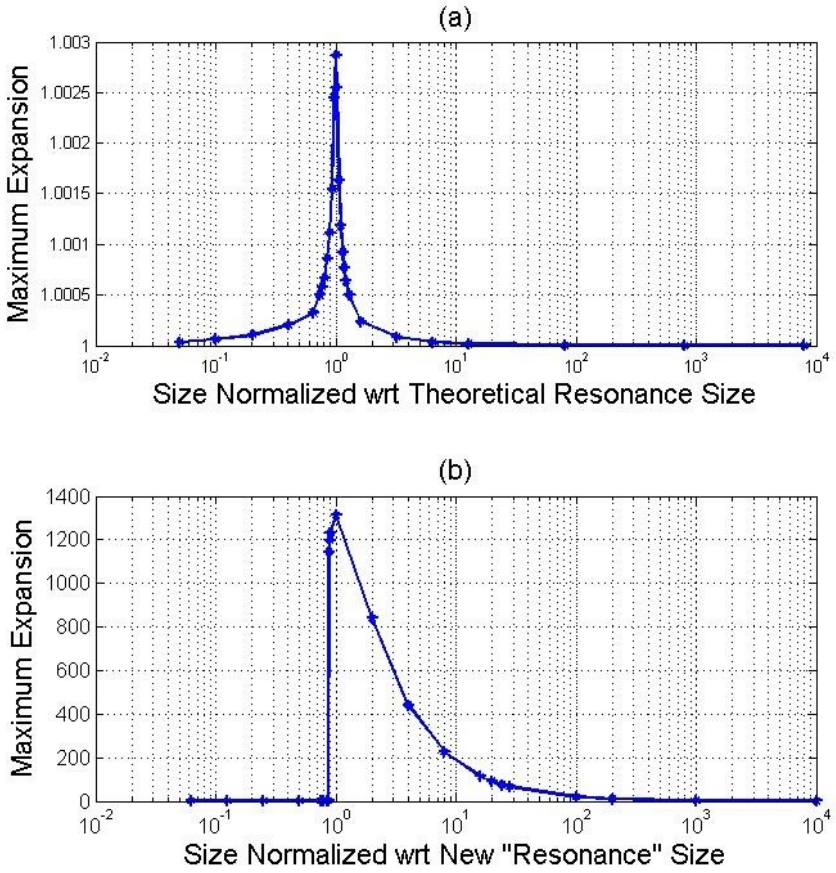

Figure 6.1: A range of initial radii is shown on a log scale normalized with respect to the theoretical resonance size 3.704 microns (a) and the simulated optimal seed size 2.9932 microns (b.) The maximum expansion of these radii is shown on a linear scale, also normalized with respect to each individual input. The frequency was 1 MHz and the pressure amplitude was 100 Pa.

While the results can provide some insight into the resonance behavior of bubbles, or technique did have several limitations. First, bubble to bubble interaction can impact resonance behavior [30, 31] and in this study a single bubble was tested. In reality a large number of bubbles would be present. Many factors arise when dealing with numerous bubbles such as the spacing between the bubbles, bubble size, and asymmetric coupled collapse of the bubbles. Another possible limitation would be the assumptions made of the

bubble during its expansion and collapse. For example, the bubble's surface tension remained constant throughout the simulations. While this assumption is true for larger bubbles, it may not be true for smaller ones. However, surface tension has been shown to be constant for nanoscale bubbles [32]. A reason the research did not consider testing higher pressures was that the physics might change as the bubble size continued to drop. This is an unfortunate limitation considering higher pressure amplitudes, up to 20 MPa, would have greater applicability in some applications such as ultrasound histotripsy [4, 33, 34, 35, 36, 37]. Nonlinear propagation also affects the system and its unaccountability limits our model, and as noted, we used only linear acoustic waves to excite the bubbles. Nonlinear distortion of the wave would be present especially at the higher pressure amplitudes. Nonlinear distortion will result in an asymmetric waveform with the peak compressional pressure becoming significantly larger than the peak rarefractional pressure. At even higher pressures, shock waves can also appear in the waveform. Due to the nonlinear nature of bubble dynamics, nonlinear distortion/shock formation is likely to have an impact on the bubble response as well.

A look at the frequency dependence on size was also an area of interest during the study. Previous works [6, 7] have noted a strong inverse dependency between frequency and resonant bubble size; as the frequency increases the bubble size decreases. This phenomenon can be clearly seen in Figure 6.2 at the left hand side of the graph. The interesting and new effect was seen at high pressure amplitudes. As the pressure increased the bubble becomes more dependent on the pressure than on the frequency. This shift begins at pressure amplitudes where transient cavitation starts to occur. The conclusion is that at higher pressure

amplitudes where inertial cavitation occurs the active bubbles are less dependent on the frequency of excitation.

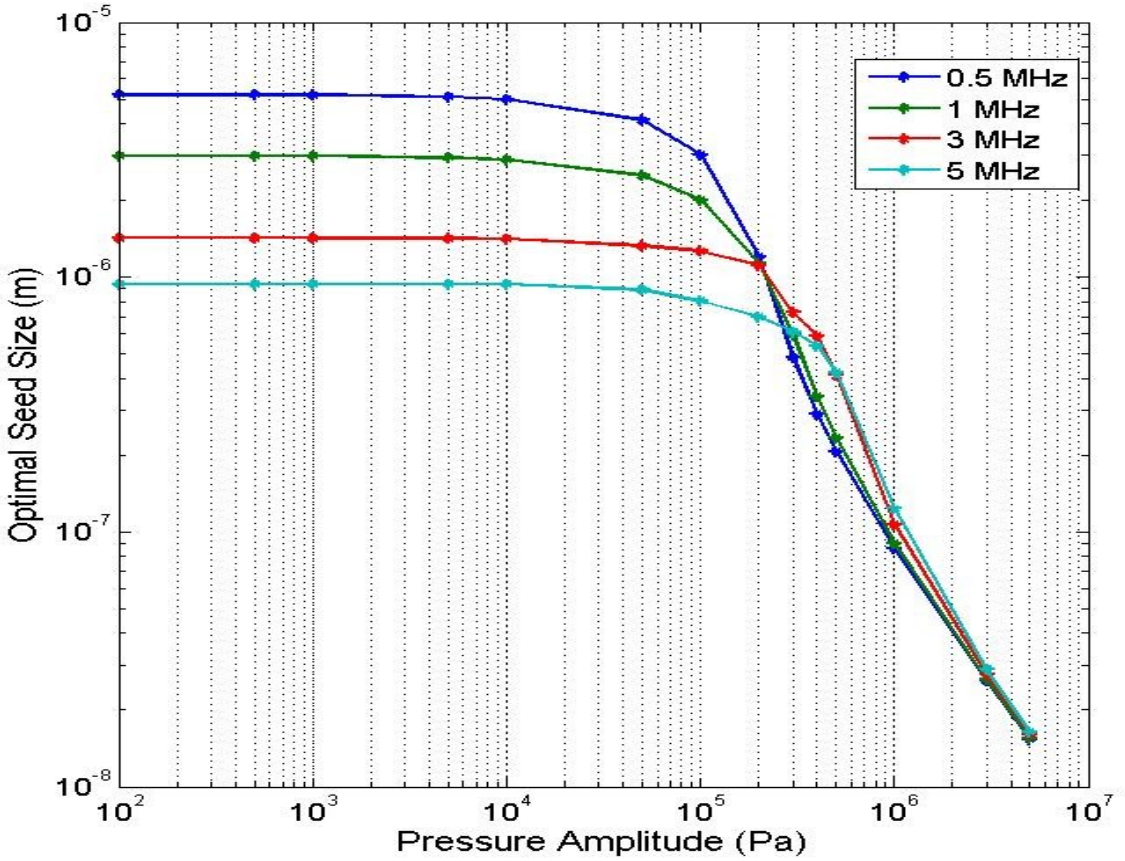

Figure 6.2: Plot shows bubble behavior under four frequencies: 0.5, 1, 3, and 5 MHz. The strong frequency dependence decreases as the pressure amplitude reaches levels where inertial cavitation occurs.

APPENDIX A: DERIVATION OF AVERAGE TIME RATE OF CHANGE IN MOLES OF GAS[6]

Define new variables depending on previously defined terms.

$$h = \frac{1}{3} \quad - \tag{A.1}$$

$$\partial \quad \partial = \quad - \tag{A.2}$$

$$\tau = \int_0^t \tag{A.3}$$

Substitute newly defined variables into the original Flick's diffusion equation

$$\left(\quad \right) \quad \frac{\partial}{\partial} \tag{A.4}$$

with the following boundary conditions

$$\begin{aligned} &U(h,0) = \\ &\lim_{h\to\infty} \frac{\partial}{\partial} - \\ &\frac{\partial}{\partial} \quad - \quad - \end{aligned} \tag{A.5}$$

The boundary condition at $r=R$ or $h=0$ is that $C=C_s$. Henry's Law states that the concentration of gas dissolved in a liquid is directly proportional to the partial pressure of the

gas above that liquid. Therefore, $C_s = k^{-1}p_g$ where ‘k’ is Henry’s constant. The concentration at saturation is given by $C_0 = k^{-1}P_0$ and $C_s = k^{-1}p_g/P_0$. Since it has been assumed that the number of moles remains approximately constant the ideal gas law for an isothermal process can be used giving $p_g R^3 = R_n^3 p_n$ where the subscript ‘n’ stands for the equilibrium values. Using these relationships C_s can be redefined as

$$C_s = \frac{P}{P_0}\left(\quad \right) \qquad \left(\quad \right) \tag{A.6}$$

and the equilibrium relationship of $p_n = P_0 + 2\sigma/R_n$ can be used to conveniently define a new variable $C_{s,n}$.

$$C_{s,n} = \quad + \tag{A.7}$$

Using Eq. A.7 and third boundary condition the partial derivative of *U* with respect to *h* can be rewritten as

$$\frac{\partial}{\partial} \quad - \quad \left(\quad \right) \tag{A.8}$$

It is assumed that a solution may be formed a series of consecutive approximations. *U* can be written as $U = U_0 + U_1 + U_2 + \ldots$, where U_n contains h/R^3 to the n^th power.

$$\frac{\partial}{\partial} - \quad \partial \quad -$$

$$\frac{\partial}{\partial} - \quad - - \quad \partial \quad = - \qquad \text{(A.9)}$$

$$\frac{\partial}{\partial} - \quad - - \quad \partial \quad - \left(\quad \right)$$

The quantity of interest is the flux of gas at the bubble wall shown by *J*.

$$J = - \quad \partial \quad - - \quad \partial \quad - \qquad \text{(A.10)}$$

This expression is integrated over the surface of the bubble to give the rate of change, n, the number of moles of gas in the bubble:

$$\frac{dn}{dt} = \quad \partial \quad - \qquad \text{(A.11)}$$

From the definition of r and the diffusion equation we can see that

$$\frac{dn}{dt} = \quad \partial \qquad \text{(A.12)}$$

Finally with integration with respect to ‘r’ and the change in ‘n’:

$$\Delta \equiv \quad - \quad = \qquad \text{(A.13)}$$

The zero order and first order solution must be solved to retrieve each change in 'n.' Using the boundary conditions stated in (A.5) the zero order solution can be found using a simple Laplace transform shown below.

$$\Delta = - \int_0^{\tau} \qquad (A.14)$$

The first order solution is much more complicated to solve. Initially the first order equation from (A.9) is used in pairing with the previous initial conditions. The equation requires the Green's function shown in (A.15) to solve the function.

$$g(h,\tau \quad \tau = \quad - \quad \times \left[\qquad \right] \qquad (A.15)$$

Using the general Green's function the first order term $U_{1,}$ can be found and in turn used to find the first order correction term Δ_1. In Eq. A.16 there are no limitations on the functions R or F.

$$\Delta = \int_0^{\tau} \qquad \int \qquad \left[\qquad \right] \qquad (A.16)$$

After solving for the correction terms in both the zero and first order cases the change in number of gas moles in the bubble as a function of 'τ' by simply adding them together. This general solution provides more than the needed amount of information for the frequency of sound field that is relevant to the cases involved. One simplification made was to assume that this bubble would be in a relatively 'high frequency' scenario. This cause the

dimensionless ratio of $(D/\omega)^{1/2}/R_n$ to be negligible. To complete this derivation $R(t)$ is period with the bubble and T_b is a small integral multiple of the acoustic field. F_0 is given by $F_0 = (1/\tau_0)\int_0^{\tau_0} F(\tau)d\tau$ which is the average of $F(\tau)$ over one period. τ_0 represents the value of τ for one period of $t=T_b$.

$$F_0 = \frac{1}{\tau} \int_{0}^{T_b} \qquad \left(\qquad \right) \tag{A.17}$$

Where the functions A and B are dependent over T_b as shown below,

$$A = \frac{1}{T_b} \int_{0}^{T_b} \qquad \tag{A.18}$$

$$B = \frac{1}{T_b} \int_{0}^{T_b} \left(\qquad \right)$$

Using the functions A and B shown in (A.18) and the difference of 'n' values as shown in (A.19) one can take the time derivative to see the average rate of change in 'n' in reference to the zero and first order solutions shown in (A.20).

$$n - \quad = \qquad + \qquad \left(\qquad \right) \tag{A.19}$$

$$\frac{dn}{dt} = \left[\qquad \right] \tag{A.20}$$

APPENDIX B: DERIVATION OF RAYLEIGH-PLESSET EQUATION IN TERMS OF BUBBLE RADIUS

The Rayleigh-Plesset equation is an addition to the Rayleigh [18] equation taking into account the surface tension and viscosity. The derivation for the equation will be completed making the same assumptions that the gas bubble is spherical in shape and has a wavelength sufficient for rectified diffusion. The bubble will also be submerged in a sizable liquid with an acoustic field acting upon it as an external force.

The liquid incompressibility cause the velocity to fall off as an inverse square law which gives a relationship between the velocity *u(r,t),* the bubble radius *R(t)* and the bubble wall velocity *R(t)/dt.* This change is bubble radius produces the pressure differences at the center of the gaseous bubble. The difference in work done along with the pressure at the bubble wall equals the kinetic energy in the liquid shown by Eq. (B.2).

$$u(r,t) = \frac{R^2(t)}{r^2(t)} \frac{dR(t)}{dt} \tag{B.1}$$

$$KE = \frac{1}{2} \int_{r=}^{\infty} \frac{d^2R}{dt^2} \tag{B.2}$$

After rearranging this kinetic energy equation, and differentiating with respect to *R,* it can be seen that the term on the left of Eq. (B.3) is the result of the difference in work done at the bubble wall and very far from the bubble wall.

$$p_i - \quad = \left(\qquad \left(\quad \right) \right) \tag{B.3}$$

Since P_∞ is the sum of the state and driving components Eq. (B.3) can be rewritten as the known Rayleigh-Plesset equation shown below.

$$R\frac{d^2R}{dt^2} + 2\left(\quad \right) \qquad - \quad + \quad \frac{1}{c}\frac{dR}{dt} \tag{B.4}$$

APPENDIX C: DERIVATION OF GILMORE FORMULATION FOR BUBBLE DYNAMICS

Gilmore [21] starts by using the basic flow relations of a spherical bubble, modeling as it grows and collapses in an infinite liquid. This method neglects any asymmetric motions the bubble might undergo during cavitation. Due to spherically symmetric liquid flow, the velocity vector, $\bar{u}$, can be written as negative the gradient of the velocity potential, ϕ, hence the equation of motion as written in Eq. C.1:

$$\frac{\partial}{\partial} \quad \nabla \quad + \quad \circ \qquad \qquad \circ \tag{C.1}$$

$$\nabla \cdot \quad = \quad \tag{C.2}$$

The conservation of mass problem can be used to transform the gradient dot the vector velocity shown in Eq. C.2. Eq. C.2 allows the viscosity term in Eq. C.1 to be ignored and the integration over the pressure field can be completed provide a couple assumptions. The first is that the pressure at infinity is a constant, and when the pressure is at infinity the velocity and its potential can be dismissed. The second assumption is that the liquid density, ρ, can be written in terms of pressure. The quantity H(p) is the enthalpy difference between the pressure at the bubble wall and the pressure at infinity. After making the assumptions and substituting Eq. C.3 into C.1 and integrating the equation a new relationship can be seen in Eq. C.4.

$$H(p) = \int_{P_\infty}^{P(R)} \frac{dp}{\rho} \tag{C.3}$$

$$-\frac{\partial \phi}{\partial t} + \frac{u^2}{2} = \int_{P_\infty}^{P(R)} \frac{dp}{\rho} \tag{C.4}$$

Assuming that the sonic wave speed does not vary significantly from its speed at infinity, c_∞, Eq. C.5 can be used to express the velocity potential for diverging spherical sound waves. Defining 'r' as the distance from the center of the bubble and 'f' as a function Eq. C.4 can be rewritten in C.5.

$$\phi = \frac{1}{r} f\left(t - \frac{r}{c}\right) \tag{C.5}$$

$$r\left(H + \frac{u^2}{2}\right) = f\left(t - \frac{r}{c}\right) \tag{C.6}$$

$$\frac{\partial}{\partial t}\left[r\left(H + \frac{u^2}{2}\right)\right] + c\frac{\partial}{\partial r}\left[r\left(H + \frac{u^2}{2}\right)\right] = 0 \tag{C.7}$$

$$r\frac{dH}{dt} + \frac{dr}{dt}H + \frac{dr}{dt}\left(\frac{u^2}{2}\right) + c\left(H + \frac{u^2}{2}\right) + cr\frac{\partial}{\partial r}\left(H + \frac{u^2}{2}\right) = 0 \tag{C.8}$$

To obtain equations C.7 and C.8 it is assumed that $r(H + u^2/2)$ is propagating through with the velocity of (c + u.) The equation is simply written in terms of particle velocity and expanded, as seen in Eq. C.8.

In the spherical, symmetric, bubble cavitation formulation Eq. C.1 can be rewritten as the derivative of the velocity with respect to time set equal to the negative value of the partial derivative of the enthalpy with respect to distance, 'r.' Neglecting the viscosity, Eq. C.2 can be written as follows:

$$\frac{\partial}{\partial} \quad -\frac{1}{c^{-}}\frac{dH}{dt} \tag{C.9}$$

Using relationships $c^2=dp/d\rho$ and $dp/\rho=dH,$ and substituting into C.8 one can see the formulation becomes a relationship between the velocity and pressure fields.

$$r\frac{\partial}{\partial}\left(\quad\right)\quad\left(\quad\right)\qquad\left(\quad\right)\qquad\left(\qquad\right) \tag{C.10}$$

The spherical flow particle derivative can be found by eliminating the derivatives with respect to 'r.' Eq. C.9 and the Eq. C.11 the particle relationship for spherical flow can be seen in Eq. C.12.

$$\frac{du}{dt} = -\frac{\partial}{\partial} \tag{C.11}$$

$$r\frac{dH}{dt}\left(\quad\right)\quad\left(\quad\right)\qquad\left(\quad\right)\qquad\left(\quad\right) \tag{C.12}$$

Gilmore justifies this result that Eq. C.12 agrees with the numerical solution of $u/c=2.2.$ The relationship between the fluid equations and the bubble wall motion are easily connected. As the bubble cavitates it is in the path of Eq. C.12. Using the fluid equation at *'r'* at the bubble wall (R) and dividing by C*:*

$$RU\frac{dU}{dR}\left(\qquad\right)\qquad\left(\qquad\right)\quad\left(\qquad\right)\qquad\left(\qquad\right)\qquad\text{(C.13)}$$

APPENDIX D: DERIVATION OF LINEAR RESONANCE FREQUENCY EQUATION[7]

For small bubble oscillations undergoing stable cavitation in a low intensity acoustic field the linear value of the resonance frequency can be derived by making the equation of motion linear. The assumptions are that the amplitude of incoming wave would be much smaller that the ambient pressure. Starting with general Keller-Herring [K-H] equation, as shown in Eq. 11, it can be rewritten in terms of pressure, shown below.

$$P(R) = \left(\right)\left(\right) \cdot \left(\right) \cdot R - \quad \text{(D.1)}$$

Parameters in Eq. D.1 are defined the same as the previous equation in this paper. Some new parameters are introduced in the above equation; μ is the viscosity of the bubble shell, χ is the shell elasticity parameter, ε as the shell thickness, and Γ is the polytropic exponent for the gas inside the bubble (air).

Using the original K-H equation given in Chapter Two (Eq. 11) and Eq. D.1the relationship $R(t)=R_0(1+x(t))$ where $-1 \leq x \leq 1$ works out to be:

(D.2)

To simplify approximations must be made.

(D.3)

To achieve the above simplification a constraint of bubbles that have a radius much greater than the specifications shown in Eq. D.4:

$$\frac{4\mu}{\rho} + \rho \ll \qquad \text{(D.4)}$$

Next administer constants to the set of parameters in front of ‘x’ and the first derivative of ‘x,’ where β and ω_0^2 are as follows:

$$\ddot{\quad} \quad \dot{\quad} \quad = - \frac{P \sin(\omega \quad \quad \omega}{\rho} - \frac{\omega}{\rho}$$

$$\beta = \left(\quad \right) \quad + \quad \quad - \quad \quad \text{(D.5)}$$

$$\omega = \frac{2\Gamma}{\rho} \left(\quad \right)$$

By using the simple relationship of frequency and angular frequency the resonant frequency can be solved for shown in Eq. D.6:

$$f_0^{lin} = \frac{1}{2\pi} \sqrt{\frac{2\Gamma}{\rho} \left(\quad \right)} \quad \text{(D.6)}$$

Eq. D.6 looks a little different from Eq. 12 because in this thesis work the shell elasticity parameter, χ, was not taken into account.

APPENDIX E: MATLAB CODE

E.1 Maximum Bubble Radius Function

This function returns the maximum bubble radius before its initial collapse altered slightly to catch the collapse when it reaches 0.999 times the initial radius.

```
function [out_min_value]=max_iradbigelow(irad,freqin,pampin,cycles)


% freqin= frequency in Hz that the ultrasound pulse is driven at
% pampin= the pressure amplitude in Pa of the bubble
% irad= initial bubble radius in m
% cycles= the number of times desired for the bubble to rise and collapse

%C     P(1)=EQUILIBRIUM BUBBLE RADIUS
%C     P(2)=SURFACE TENSION
%C     P(3)=EXPOSURE FREQUENCY
%C     P(4)=EXPOSURE PRESSURE AMPLITUDE
%C     P(5)=AMBIENT PRESSURE
%C     P(6)=POLYTROPIC EXPONENT
%C     P(7)=RATIO OF SPECIFIC HEATS
%C     P(8)=DENSITY OF GAS IN CAVITY
%C     P(9)=THERMAL CONDUCTIVITY OF GAS
%C     P(10)=FLUID VISCOSITY
%C     P(11)=LIQUID DENSITY
%C     P(12)=SPEED OF SOUND IN LIQUID
%C     P(13)=INITIAL PRESSURE OF GAS IN CAVITY
%C     P(14)=EQUILIBRIUM VAPOR PRESSURE OF LIQUID
%C     P(15)=LATENT HEAT OF VAPORIZATION OF LIQUID
%C     P(16)=SPECIFIC HEAT OF GAS AT CONSTANT VOLUME
%C     P(17)=MOLECULAR WEIGHT OF GAS
%C     P(18)=ABSOLUTE TEMPERATURE OF THE LIQUID
%C     P(19)=SPEED OF SOUND IN GAS
%C     P(20)=VAPOR PRESSURE OF LIQUID AT EQUILIBRIUM

%C  Last change:  CCC   25 Apr 2008   11:55 am
%C  THIS IS INTERACTIVE PROGRAM CBD.FOR

%C       WRITTEN BY  CHARLES C. CHURCH
%C                   National Center for Physical Acoustics
%C                   University of Mississippi
%C                   1 Coliseum Drive
%C                   University, MS 38677
%C                   662-915-6517 (OFFICE)
```

```
%C                662-915-5643 (FAX)

%C       REVISED BY  KELSEY CARVELL
                                 Electrical and Computer Engineering
                                 Iowa State University of Science and Technology
                                 2201 Coover Hall
                                 Ames, IA 50010

%C  IT CALCULATES THE RESPONSE OF BUBBLES TO A SINE WAVE.  THE PHASE OF
%C  THE ACOUSTIC PRESSURE IS NEGATIVE INITIALLY.  THIS MAY BE REVERSED
%C  BY ENTERING A NEGATIVE VALUE FOR PRESSURE.  ALL UNITS ARE CGS.
%C  THE PROGRAM SOLVES THE GILMORE-AKULICHEV FORMULATION FOR BUBBLE
%C  DYNAMICS USING A FOURTH ORDER RUNGE-KUTTA ALGORITHM.  THE OUTPUT
%C  CONSISTS OF FOUR COLUMNS: TIME, RADIUS, THE VELOCITY OF THE BUBBLE
%C  WALL AND ACOUSTIC PRESSURE, ALL IN NONDIMENSIONAL FORM.  THE
%C  NORMALIZATION PARAMETERS USED FOR THIS ARE: ACOUSTIC PERIOD FOR
%C  TIME, EQUILIBRIUM BUBBLE RADIUS FOR RADIUS, (LIQUID DENSITY/SPEED OF
%C  SOUND)^0.5 FOR VELOCITY AND AMBIENT PRESSURE FOR ACOUSTIC PRESSURE.
%C  THE INITIAL VALUE FOR "STEPS PER UNIT TIME" SHOULD BE 1000 OR MORE,
%C  THE PROGRAM WILL THEN ADJUST THIS VALUE AS THE CALCULATION PROCEEDS.

%C  NACPR IS THE VARIABLE FOR THE ACOUSTIC PRESSURE
%C  DNACPR IS THE VARIABLE FOR THE DERIVATIVE OF THE ACOUSTIC PRESSURE



freq=freqin;
R_bubble_res=irad;
f=freq;
pamp = -pampin;
time=(1/f)*(0:0.01:cycles);
p=pamp*sin(2*pi*f*time);
p=-p/0.1;
t_norm=time*f;
R_bubble_eq = 1*(100*R_bubble_res); %Equlibrium Bubble radius in cm


P(1)=R_bubble_eq; %Equlibrium Bubble radius cm
P(2)=6.8e1;
P(3)=f;
%P(4)=0
P(5)=1.01e6;
P(6)=.14e1;
P(7)=1.4;
P(8)=1.18e-3;
P(9)=2.612e3;
P(10)=1e-2;
P(11)=1.0;
P(12)=1.50e5;
P(13)=1.778e6;
P(14)=2.33e4;
P(15)=2.09e10;
P(16)=7.201e6;
```

```
P(17)=2.8e1;
P(18)=2.93e2;
P(19)=3.31e4+6.0e1*(P(18)-2.73e2);
P(20)=2.33e4;
TPI=2*pi;
PBAR = 0;
ACUNUM = 20000;%input('ENTER THE NUMBER OF STEPS PER UNIT TIME (>10000):');

%Choose gas for calculations.
GASNUM = 1;%input('WHAT GAS IS IN THE BUBBLE?\n 1) Air, 2) Argon, 3) Xenon, 4) 50:50 Air:C3F8,
5) C3F8, 6) C4F10, 7) C5F12 \n Enter a Number: ');

if (GASNUM==1)
   GNAME='100% AIR'
   P(6)=.14e1;
   P(7)=1.4;
   P(8)=1.2928e-3;
   P(9)=2.612e3;
   P(16)=7.201e6;
   P(17)=2.88e1;
   P(19)=3.31e4+6.0e1*(P(18)-2.73e2);
elseif GASNUM == 2
   GNAME='100% ARGON'
   P(6)=.16666e1;
   P(7)=1.6666e0;
   P(8)=1.783e-3;
   P(9)=1.79e3;
   P(16)=3.126e6;
   P(17)=3.99e1;
   P(19)=3.19e4;% ARGON';
elseif GASNUM == 3
   GNAME='100% XENON'
   P(6)=.16666e1;
   P(7)=1.6666e0;
   P(8)=5.85e-3;
   P(9)=0.56e3;
   P(16)=9.60e5;
   P(17)=1.313e2;
   P(19)=1.76e4;
elseif GASNUM == 4
   P(6)=1.243e0;
   P(7)=1.243e0;
   P(8)=4.608e-3;
   P(9)=1.874e3;
   P(16)=7.306e6;
   P(17)=1.085e2;
   GNAME='50% AIR & 50% C3F8,'
elseif GASNUM == 5
   P(6)=1.087e0;
   P(7)=1.087e0;
   P(8)=8.003e-3;
   P(9)=1.1350e3;
   P(16)=7.41e6;
   P(17)=1.8802e2;
```

```
   GNAME='100% C3F8,'
elseif GASNUM == 6
   P(6)=1.069e0;
   P(7)=1.069e0;
   P(8)=9.935e-3;
   P(9)=9.68e2;
   P(16)=7.55e6;
   P(17)=2.38e2;
   GNAME='100% C4F10,'
elseif GASNUM == 7
   P(6)=1.057e0;
   P(7)=1.057e0;
   P(8)=1.139e-2;
   P(9)=9.68e2;          % THIS VALUE IS FOR C4F10
   P(16)=7.55e6;          % THIS VALUE IS FOR C4F10
   P(17)=2.88e2;
   GNAME='100% C5F12,'
else
   error('Wrong number entered for gas type!')
end

P(13)=P(5)+2e0*P(2)/P(1)-P(20);


R(1) = P(1)%input('ENTER THE INITIAL BUBBLE RADIUS IN cm:');
R(1) = R(1);
U(1) = 0;%input('ENTER THE INITIAL BUBBLE VELOCITY IN cm/s:');
U(1)= U(1);

R(1)=R(1)/P(1);

NVEL=sqrt(P(11)/P(5));
U(1)=U(1)*NVEL;

if (GASNUM>1)
   P(19)=P(19)*P(18)/2.93e2;
end

%C
%C  THIS NEXT PART CALCULATES A VALUE FOR THE POLYTROPIC EXPONENT
%C  A LA PROSPERETTI, IF YOU WANT IT TO.
%C

ANS = 'n';%input('DO YOU WANT TO CALCULATE A MORE EXACT VALUE FOR THE POLYTROPIC
EXPONENT? ','s');

if (ANS=='Y' || ANS=='y')
   DG=P(9)/P(8)/P(16);
   G1=7.555901328e-8*P(17)*P(3)*DG/P(18)/P(7);
   G2=TPI*P(3)*P(1)*P(1)/DG;

   if (G1>(5e-2)) || ((G1*G2)>5e-2)
```

```
        DL=P(9)/(P(8)*P(16)*P(7));
        BIGX=P(1)*sqrt(2*TPI*P(3)/DL);
        E1=exp(BIGX);
        E2=exp(-1*BIGX);
        E3=(E1-E2)*.5;
        E4=(E1+E2)*.5;
        E5=sin(BIGX);
        E6=cos(BIGX);
        T=3*(P(7)-1);
        X2=BIGX*BIGX;
        BT=X2*(E4-E6)+T*BIGX*(E3-E5);
        BT=T*(BIGX*(E3+E5)-2*(E4-E6))/BT;
        BT=P(7)/(1+BT*BT);
        P(6)=T*(E3-E5)/((E4-E6)*BIGX);
        P(6)=BT/(1+P(6));
    else
        K1=sqrt(G1*G2);
        K2=(P(7)-1)*G1/(2*P(7));
        K3=sqrt(P(7)*G2/2);
        E1=2*K1*K2;
        E2=exp(E1);
        E3=exp(-1*E1);
        SINH1=(E2-E3)/2;
        COSH1=(E2+E3)/2;
        K4=SINH1/(COSH1-cos(2*K1));
        K5=sin(2*K1)/(COSH1-cos(2*K1));
        E4=2*K3*(1-K2);
        E5=2*K3*(1+K2);
        E6=exp(E4);
        E7=exp(-1*E4);
        SINH2=(E6-E7)/2;
        COSH2=(E6+E7)/2;
        COS2=cos(E5);
        K6=SINH2/(COSH2-COS2);
        K7=sin(E5)/(COSH2-COS2);
        BIGA=K1*(K2*K4+K5)-1;
        BIGB=K1*(K4-K2*K5);
        BIGC=(E4*K6+E5*K7)/2-1;
        BIGD=(E5*K6-E4*K7)/2;
        K8=4*K2;
        K9=2*G1/P(7);
        PT1=2*BIGB+K8*BIGC-K9*BIGA;
        PT2=K8*BIGD-2*BIGA-K9*BIGB;
        RLPH=(K9-K8)*PT1+2*PT2;
        RLPH=RLPH/(PT1*PT1+PT2*PT2);
        P(6)=P(7)*G1*G2*RLPH/3;
    end

end

for I=1:20

end
```

```
TIMEN=P(1)*sqrt(P(11)/P(5));

np_wav = p/P(5);

for ti=2:(length(np_wav)-1)
   npD_wav(ti)=(np_wav(ti+1)-np_wav(ti-1))/(2*(time(2)-time(1)));
end

npD_wav(length(np_wav))=(np_wav(length(np_wav))-np_wav(length(np_wav)-1))/(time(2)-time(1));
npD_wav(1)=(np_wav(2)-np_wav(1))/(time(2)-time(1));

npD_wav=npD_wav*TIMEN;

TIME=0;

%ANS = input('DOES TIME START AT T=0?  ','s');

%if (ANS=='n')||(ANS=='N')
%    TIME = input('WHEN DOES IT BEGIN, IN ACOUSTIC PERIODS?  ');
%end

%CYCPRS = input('AFTER HOW MANY CYCLES DOES THE PRESSURE END?  ');
%CYCANS = input('AFTER HOW MANY CYCLES SHOULD CALCULATIONS END?  ');
%CYCNUM = input('HOW MANY POINTS SHOULD BE COLLECTED PER CYCLE?  ');

TCHANG=(time(2)-time(1))/TIMEN;%1/CYCNUM/(P(3)*TIMEN);
DIG=1 + TIME;
IDIG=DIG;
DIGLOW=IDIG;
NCYCAN=max(t_norm);

for I=1:201
   TMAX(I)=0;
   TMIN(I)=0;
   RMAX(I)=0;
   RMIN(I)=2e3;
end

OLDR=R(1);
LILV2=P(12)*P(12)*P(11)/P(5);
CAPA=LILV2/7;
CAPK=CAPA^(1/7)*7/6;
SMCAPK=CAPK*6/7;
CAPA1=CAPA-1;
EXPO=6/7;
EXPON=-1/7;
D=2*P(2)/(P(1)*P(5));
V=4*P(10)/(P(1)*sqrt(P(5)*P(11)));
G3=3*P(6);
G31=G3+1;
VAPOR=P(20)/P(5);
```

```
BIGD1=1+D-VAPOR;
GCON=P(1)/(NVEL*NVEL);
CCON=P(12)*P(12);
PCON=P(5)/1.01e6;
ERGEXP=14/6;
NFREQ=TPI*P(3)*TIMEN;

%DNPRAP=NPRAMP*NFREQ/0; %%%%%%%%%%%%%%%%%%%%%%%%%%%%%%%%%%%%

TIME=TPI*TIME/NFREQ;
OLDTIM=TIME;
CYCCON=NFREQ/TPI;
INV6=1/6;
DTIME=1/ACUNUM;
SIXA=DTIME*INV6;
NN=0;
NNN=0;
ULEAST=0;
TLEAST=0;
EINTOT=0;
ESCTOT=0;
TIMTOT=0;
CYC7=7/CYCCON;
CYC10=10/CYCCON;

NACPR = interp1(2*pi*t_norm,np_wav,NFREQ*TIME,'linear');
%NACPR=NPRAMP*sin(NFREQ*TIME); %%%%%%%%%%%%%%%%%%%%%%%%%%%%

CYCLES=TIME*CYCCON;

ti_out=1;
time_out(ti_out)=CYCLES;
radius_out(ti_out)=R(1);
velocity_out(ti_out)=U(1);
pbar_out(ti_out)=PBAR;

R(2)=R(1);
U(2)=U(1);

goto75 = 'y';

while (goto75 == 'y')
   goto75 = 'n';
   U(1)=U(2);  %%%LINE 75
   R(1)=R(2);
   XN=0;
   XELL=0;
   XKAY=0;

   for K=1:4
      OMEGAT=NFREQ*(TIME+XN/ACUNUM);
```

```
        if OMEGAT<max(2*pi*t_norm)
           NACPR = interp1(2*pi*t_norm,np_wav,OMEGAT,'linear');
           DNACPR = interp1(2*pi*t_norm,npD_wav,OMEGAT,'linear');
        else
           NACPR = 0;
           DNACPR = 0;
        end
        %NACPR=NPRAMP*sin(OMEGAT);
%%%%%%%%%%%%%%%%%%%%%%%%%%%%%%%%%%%%%%%%%%%%%%%%%%%%%%%%%%%%%%%%%%%%%%%%%%%%%%%%%%%%

        %DNACPR=DNPRAP*cos(OMEGAT);
%%%%%%%%%%%%%%%%%%%%%%%%%%%%%%%%%%%%%%%%%%%%%%%%%%%%%%%%%%%%%%%%%%%%%%%%%%%%%%%%%%%%

        NEWR=R(1)+XKAY;
        INVNR=1/NEWR;
        NEWU=U(1)+XELL;
        A1=abs(BIGD1*INVNR^G3-(D+V*NEWU)*INVNR+VAPOR+CAPA1);

        %C  THIS IS THE EXPRESSION FOR THE ENTHALPY,H
          H=CAPK*(A1^EXPO-(CAPA-NACPR)^EXPO);
        %C  MOST IS THE PART OF DH/DT ON THE RIGHT SIDE OF THE EQ. FOR DU/DT
          B1=G3*BIGD1*NEWU*INVNR^G31;
          B2=(D+V*NEWU)*NEWU*INVNR^2;
          MOST=SMCAPK*(A1^EXPON*(B2-B1)+(CAPA-NACPR)^EXPON*DNACPR);  %CHECK
          VBAR=sqrt(LILV2+6*H);
          INVBAR=1/VBAR;
          UV=NEWU*INVBAR;
          A2=1-UV;
          P1=(UV/2-1.5)*NEWU*NEWU;
          P2=(1+UV)*H;
          P3=NEWR*A2*INVBAR*MOST;
          P4=A2*(NEWR+SMCAPK*V*(A1^EXPON)*INVBAR);
        %C  THIS IS THE EQUATION OF MOTION
          ELL(K)=(P1+P2+P3)/P4;
          KAY(K)=U(1)+XELL;
          XN=XN+.5;

          if K==2
             XN = 0.5;
          end

          XELL=XN*DTIME*ELL(K);
          XKAY=XN*DTIME*KAY(K);
    end

    R(2)=R(1)+(KAY(1)+2*(KAY(2)+KAY(3))+KAY(4))*SIXA;
    FN=ELL(1)+2*(ELL(2)+ELL(3))+ELL(4);
    U(2)=U(1)+FN*SIXA;

    if (U(2)<ULEAST)
        TLEAST=TIME+DTIME;
        ULEAST=U(2);
        %TLEAST*CYCCON
```

```
end

M1=abs(KAY(2)-KAY(3));
M2=abs(KAY(1)-KAY(2));
MPLUS=M1+M2;

if (MPLUS<1e-12)
   ACUNUM=ACUNUM*.5;
end

if (MPLUS >= 2e-8)  %Go to 82

   goto=0;

   if M2>0
      M3=abs(M1/M2);
   elseif M2==0;
      M3=0;
      goto=81;  %Goto 81;
   end

   if (goto~=81)
      if (M3>3e-2)
         ACUNUM=ACUNUM*1.2;
      end
      NN=NN+1;
      if NN<6
         goto=82; %Goto 81;
      end
   end

   if goto~=82
      if (M3<1e-2)
         ACUNUM=ACUNUM*.5;
      end
      NN=0;
   end
end

%LINE 82
if (ACUNUM<2000)
   ACUNUM=2000;
end

if (TIME>=CYC7)&&(TIME<=CYC10)
   A1=abs(BIGD1/(R(2)^G3)-(D+V*U(2))/R(2)+VAPOR+CAPA1);
   H=CAPK*(A1^EXPO-(CAPA-NACPR)^EXPO);
   CAPG=GCON*R(2)*(H+5D-1*U(2)*U(2));
   PBAR=CAPA*(0.25+0.75*sqrt(1+8*CAPG/CCON))^ERGEXP-CAPA;
   PBAR=PBAR*PCON;
   ESCAT(2)=PBAR*PBAR;
   EIN(2)=NACPR*R(2)*R(2)*U(2);
```

```
      if NNN==1
        ESCTOT=ESCTOT+(ESCAT(1)+ESCAT(2))*DTIME*.5;
        EINTOT=EINTOT+(EIN(1)+EIN(2))*DTIME*.5;
        TIMTOT=TIMTOT+DTIME;
      end
      EIN(1)=EIN(2);
      ESCAT(1)=ESCAT(2);
      NNN=1;
    end

    TIME=TIME+DTIME;
    DTIME=1/ACUNUM;
    SIXA=DTIME*INV6;

    if (U(2)~=0)&&( (U(1)/U(2))>=0 )  %Go to 84 if not true
      if (abs(1-R(2)/OLDR)<1e-6)   %IF((DABS(1D0-R(2)/OLDR)).LT.1D-6) GO TO 75
        goto75='y';
      elseif ((TIME-OLDTIM)<TCHANG) %IF((TIME-OLDTIM).LT.TCHANG) GO TO 75
        goto75='y';
      end
    end

    if (goto75 ~= 'y')
     %Line 84
     OLDTIM=TIME;
     CYCLES=TIME*CYCCON;

     %if (CYCLES>=CYCPRS)
%%%%%%%%%%%%%%%%%%%%%%%%%%%%%%%%%%%%%%Pressure DATA
     %    NPRAMP=0.0;
     %    DNPRAP=0.0;
     %end

     %C  PBAR IS THE PRESSURE AT A DISTANCE OF 1 CM FROM THE BUBBLE CENTER
     OLDR=R(2);
     A1=abs(BIGD1/(R(2)^G3)-(D+V*U(2))/R(2)+VAPOR+CAPA1);
     H=CAPK*(A1^EXPO-(CAPA-NACPR)^EXPO);
     CAPG=GCON*R(2)*(H+5D-1*U(2)*U(2));
     PBAR=CAPA*(0.25+0.75*sqrt(1+8*CAPG/CCON))^ERGEXP-CAPA;
     PBAR=PBAR*PCON;

     ti_out=ti_out+1;
     time_out(ti_out)=CYCLES;
     radius_out(ti_out)=R(2);
     velocity_out(ti_out)=U(2);
     pbar_out(ti_out)=PBAR;

     %radius_out_max_return=max(radius_out(1:ti_out,rii));

     %if radius_out(ti_out,rii)<1 %Look for first collapse.
       %return radius_out_max_return;
```

```
    %    break
    %end



    %85   FORMAT(4E15.5)

    %     IF(CYCLES-DIG) 87,87,86 %%%%%%%%%%%%%%%%%%?????????
    %86   DIG=DIG+1D0
    %IDIG=IDINT(DIG)
    %WRITE(6,*) DIG

    if ((CYCLES-DIG)>0)
       DIG=DIG+1;
       IDIG=DIG;
       DIG
    end

    if RMAX(IDIG)<=R(2) %Go to 88
       RMAX(IDIG)=R(2);
       TMAX(IDIG)=CYCLES;
    end

    if (RMIN(IDIG)>=R(2)) %Go to 89
       RMIN(IDIG)=R(2);
       TMIN(IDIG)=CYCLES;
    end

    %if (CYCANS>CYCLES)  %Go to 75 %%%%%%
    %    goto75='y';
    %end
    (max(t_norm)>=CYCLES)
    (radius_out(ti_out)>1)
    (max(t_norm)>=CYCLES)&(radius_out(ti_out)>1)
    if ( (max(t_norm)>=CYCLES)&(radius_out(ti_out)>1))  %Go to 75 %%%%%%
       goto75='y';
    end
  end
end


ULEAST=ULEAST/NVEL;
TLEAST = NFREQ*TLEAST/TPI;

peak_collapse_velocity = ULEAST
peak_collapse_velocity_time = TLEAST

%input('Write down 2 values!');

REND=R(2)*P(1);
UEND=U(2)/NVEL;
```

```
TIMTOT=TIMTOT*CYCCON;
EINTOT=12.56637062*P(5)*P(1)*P(1)*CYCCON*EINTOT/(NVEL*P(3))/TIMTOT;
ESCTOT=P(5)*P(5)*CYCCON*12.56637062*ESCTOT/(P(11)*P(12)*P(3));
ESCTOT=ESCTOT/TIMTOT;

%WRITE(7,102) EINTOT,ESCTOT
% 102  FORMAT(' THE INPUT ENERGY IS',E13.5,' ERGS per CYCLE',/,
%     *  ' THE SCATTERED ENERGY IS',E13.5,' ERGS per CYCLE')


for I=DIGLOW:NCYCAN

   radius_bubble_max(I) = RMAX(I).*R_bubble_eq;  %Maximum bubble radius in cm.
   radius_bubble_max_time(I) = TMAX(I); %Time corresponding to max radius in periods of wave.
end

radius_bubble_MAXALL = max(RMAX).*R_bubble_eq  %Maximum bubble radius in cm.
radius_bubble_MAX_EXPAND = max(RMAX)  %Maximum bubble radius normalized to initial radius.

out_min_value=1./radius_bubble_MAX_EXPAND; %Value that is used to find the resonance size later.
%out_min_value=1./radius_bubble_MAXALL; %Value that is used to find the resonance size later.

%out_min_value=1./abs(peak_collapse_velocity); %Value that is used to find the resonance size later.

figure(1)
clf
subplot(311)
plot(t_norm,-p)
hold on
grid
xlabel('Normalized Time')
ylabel('Pressure dyne/cm^2')
axis([0 5 min(p) max(p)])
subplot(312)
plot(time_out,radius_out,'.')
hold on
grid
xlabel('Normalized Time')
ylabel('Normalized Radius')

subplot(313)
plot(time_out,velocity_out,'.')
hold on
grid
xlabel('Normalized Time')
ylabel('Normalized Velocity')
```

E.2 Search Function

This function used variables of frequency, pressure amplitude and cycles to complete a bounded search over the function in C.1 titled *max_iradbigelow.* It was written to scan initial bubble sizes searching for the maximum expansion relative to the initial size, prior to when the bubble dropped below its initial size. Finding this optimal seed size was the primary goal of the simulations. For example, if the frequency was on the 1 MHz loop and the pressure amplitude (pamp) was on the 1 MPa loop the search function would find the smallest bubble size for that particular set of input variables. This example of the code would produce twenty eight values of optimal seed sizes.

```
clear all
close all

%Goal is to find the resonance size of the bubble.

cycles=50;

%collapse_condition=0.999.*(irad) %Just for reference not used in code.

%Value of 0.5 was used for:
%    freq1MHz_lowP.mat
%    freq3MHz_lowP.mat
%    freq5MHz_lowP.mat

freq = [0.5e6 1e6 3e6 5e6] %Change in freq.

pamp = [0.0001 0.000.5 0.001 0.005 0.01 0.05 0.1 0.5 1 3 5]*1e6

fi=1
pi=1

r_theory = find_size_theory(freq(fi));


%break

for fi=1:length(freq)
```

```
    r_theory = find_size_theory(freq(fi))

    for pi=1:length(pamp)

        %max_irad(r_theory,freq(fi),pamp(pi),cycles)

                    r_sim(fi,pi)=fminbnd(@(x)max_iradbigelow(x,freq(fi),pamp(pi),cycles),r_theory/10000,r_the
                    ory*1.5,optimset('TolX',1e-10))

        save freq1_lowlowamp.mat
        %EXAMPLE: save freq1MHz_highP.mat

    end
end
```

E.3 Finding Theoretical Size

Using the Keller-Herring linearization of the bubble dynamics a theoretical resonance size was modeled. The code used a roots function to solve for the resonance size given a specific frequency. The original equation is shown in Eq. 12, Chapter 3. This was implemented into the search function to serve as a sanity check for the results as low pressure amplitudes.

```
function r_size = find_size_theory(f);
% Resonance size given bubble frequency


%Equation given in "A Numerical Investigation of the Resonance of
%Gas-filled Microbubbles: Resonance Dependence on Acoustic Pressure
%Amplitude" NOTE: the ki(shell elasticity parameter) terms were neglected



%  sigma = SURFACE TENSION
%  po    = AMBIENT PRESSURE
%  Gamma = POLYTROPIC EXPONENT of encapsulated gas
%  rho   = LIQUID DENSITY


sigma =0.068; %N/m
po=1.01e5; %Pa
Gamma =.14e1;
rho = 1000; %kg/m^3
```

```
a = (f.^2).*4.*pi.*pi;
b = 0;
c = ((-3.*Gamma.*po)./(rho));
d = ((-6.*sigma.*Gamma+2.*sigma)./(rho));

disp('Only use Real root!')

p = [a b c d]
r = roots(p)

rnum=0

for ri=1:length(r)
   if r(ri)>0
      r_size=r(ri);
      rnum=rnum+1;

      if rnum>1
         error('Too many roots!!')
      end
   end
end

fo_test=(1/(2*pi))*sqrt( (3*Gamma/(rho*r_size.^2))*(po + 2*sigma./r_size) - 2*sigma/(rho*r_size.^3) )
```

REFERENCES

[1] http://www.cancer.org/docroot/STT/STT_0.asp American Cancer Society, May 18th , 2009

[2] Parsons, J.E., Cain, C.A., Abrams, G.D. et al., **(2006)** "Pulsed cavitational ultrasound therapy for controlled tissue homogenization," Ultrasound in Medicine & Biology **32**, 115-129

[3] Xu, Z., Ludomirsky, A., Eun, L.Y. et al., **(2004)** "Controlled ultrasound tissue erosion," Ultrasonics, Ferroelectrics and Frequency Control, IEEE Transactions on **51**, 726-736.

[4] Hall TL, Cain CA, **(2005)** "A Low cost, compact, 512 channel therapeutic system for transcutaneous ultrasound surgery," International symposium on therapeutic ultrasound, S035.

[5] Young, Ronald F. Cavitation McGraw-Hill, 1989.

[6] Eller and H. G. Flynn **(1965)** "Rectified Diffusion during Nonlinear Pulsations of Cavitation Bubbles," J. of Acous. Soc. of America **37**, 493-503.

[7] MacDonald, C.A., Sboros, V., Gomatam, J. et al., **(2004)** " A theoretical study of cavitation generated by an extracorporeal shock wave lithotripter," Ultrasonics **43**, 113-122.

[8] Wu, F., Wang, Z.-B., Chen, W.-Z., Zou, J.-Z., Bai, J., Zhu, H., Li, K.-Q., Xie, F.-L., Jin, C.-B., Su, H.-B. and Goa, G.-W. **(2004)** Extracorporeal focused ultrasound surgery for treatment of human solid carcinomas: early Chinese clinical experience," Ultrasound Med. Bio. **30,** 245-260.

[9]Foley, J.L., Little, J.W., Starr III, F.L. et al., **(2004)** "Image-guided HIFU neurolysis of peripheral nerves to treat spasticity and pain." Ultrasound Med. Biol. **30**, 1199-1207.

[10] Christopher, T., **(2005)** "HIFU focusing efficiency and a twin annular array source for p prostate treatment" Ultrasonics, Ferroelectrics and Frequency Control, IEEE Transactions on **52**, 1523-1533.

[11] Fry, F.J. and Eggleton, R.C., **(1972)** "Ultrasonic device for human disease diagnosis and surgery," Technical Communication 33-37.

[12] Everbach, E.C. and Francis, C.W., **(2000)** "Cavitation mechanisms in ultrasound-accelerated thrombolysis at 1 MHz," Ultrasound Med. Biol. **26**, 1153-1160.

[13] Guzman, H. R., McNamara, A. J., Nguyen, D. X. and Prausnitz, M. R. **(2003)** "Bioeffects caused by changes in acoustic cavitation bubble density and cell concentration: a unified explanation based in cell-to-bubble ratio and blast radius," Ultrasound Med. Bio. **29,** 1211-1222.

[14] Roberts, W. W. **(2005).** "Focused ultrasound ablation of renal and prostate cancer: Current technology and future directions," Urologic Oncology: Seminars and Original Investigations **23,** 367-371.

[15] Xu, Z., Fowlkes, J. B., Rothman, E. D., Levin, A. M. and Cain, C. A. **(2005)**. "Controlled ultrasound tissue erosion: The role of dynamic interaction between insonation and microbubble activity," J. Acoust. Soc. Am. **117,** 424-435.

[16] Bigelow, T. A., Northagen, T., Hill, T. M., and Sailer, F. C. (**2009**). "The Destruction of Escherichia Coli Biofilms Using High-Intensity Focused Ultrasound," Ultrasound Med. Biol. **35**, 1026-1031.

[17] Epstein, P. S., and Plesset, M.S., **(1950)** "On the stability of gas bubbles in liquid-gas solutions," J. Chemical Physics. **18,** 1505-1509.

[18] Sboros, V., MacDonald, C. A., Pye, S. D., Moran, C. M., Gomatam, J., and McDicken, N. **(2002)** "The dependence of ultrasound contrast agents backscatter on acoustic pressure: theory versus experiments" Ultrasonics. **40** 579-583.

[19] Lord Rayleigh, **(1017) "**On the pressure developed in a liquid during the collapse of spherical cavity." Philos.Mag. **34,** 94–98.

[20] M.S. Plesset, **(1949)** "Dynamics of cavitating bubbles" J. Appl. Mech., Trans. ASME **16,** 227-282.

[21] F.R. Gilmore, **(1954)** California Institute of Technology, Hydrodynamic Laboratory Report 26-4,

[22] Church, C.C. **(1988)** "Prediction of rectified diffusion during nonlinear bubble pulsations at biomedical frequencies," J. Acoust. Soc. Am. **83**, 2210-2217.

[23] Church, C.C. **(1989)** "A theoretical study of cavitation generated by an extracorporeal shock wave lithotripter." J. Acoust. Soc. Am. **86,** 215-227.

[24] Gracewski, S.M., Miao, H. and Dalecki, D. **(2005)** "Ultrasonic excitation of a bubble near a rigid or deformable sphere: Implications for ultrasonically induced hemolysis," J. Acoust. Soc. Am. **117,** 1440-1447.

[25] Jimenez-Fernandez, J., and Crespo, A. (**2005**). "Bubble oscillation and inertial cavitation in viscoelastic fluids," Ultrasonics **43**, 643-651.

[26] Kimmel, E., Krasovitski, B., Hoogi, A., Razansky, D., and Adam, D. (**2007**). "Subharmonic Response of Encapsulated Microbubbles: Conditions for Existence and Amplification," Ultrasound Med. Biol. **33**, 1767-1776.

[27] Chatterjee, D., and Sarkar, K. (**2003**). "A Newtonian rheological model for the interface of microbubble contrast agents," Ultrasound Med. Biol. **29**, 1749-1757.

[28] Beyer, R. T. Nonlinear Acoustics Acoustical Society of America, Woodbury, NY, 1997.

[29] Holland, C. K., and Apfel, R. E. (**1989**). "An improved theory for the prediction of microcavitation thresholds," Ultrasonics, Ferroelectrics and Frequency Control, IEEE Transactions on **36**, 204-208.

[30] Allen, J. S., Kruse, D. E., Dayton, P. A., and Ferrara, K. W. (**2003**). "Effect of coupled oscillations on microbubble behavior," J. Acoust. Soc. Am. **114**, 1678-1690.

[31] Skaropoulos, N. C., Yagridou, H. D., and Chrissoulidis, D. P. (**2003**). "Interactive resonant scattering by a cluster of air bubbles in water," J. Acoust. Soc. Am. **113**, 3001-3011.

[32] Matsumoto, M., and Tanaka, K. (**2008**). "Nano bubble--Size dependence of surface tension and inside pressure," Fluid Dynamics Research **40**, 546-553.

[33] Parsons, J. E., Cain, C. A., and Fowlkes, J. B. (**2007**). "Spatial variability in acoustic backscatter as an indicator of tissue homogenate production in pulsed cavitational ultrasound therapy," Ultrasonics, Ferroelectrics and Frequency Control, IEEE Transactions on **54**, 576-590.

[34] Xu, Z., Fan, Z., Hall, T. L., Winterroth, F., Fowlkes, J. B., and Cain, C. A. (**2009**). "Size Measurement of Tissue Debris Particles Generated from Pulsed Ultrasound Cavitational Therapy - Histotripsy," Ultrasound Med. Biol. **35**, 245-255.

[35] Xu, Z., Raghavan, M., Hall, T. L., Ching-Wei, C., Mycek, M. A., Fowlkes, J. B., and Cain, C. A. (**2007**). "High Speed Imaging of Bubble Clouds Generated in Pulsed Ultrasound Cavitational Therapy - Histotripsy," Ultrasonics, Ferroelectrics and Frequency Control, IEEE Transactions on **54**, 2091-2101.

[36] Xu, Z., Raghavan, M., Hall, T. L., Mycek, M. A., Fowlkes, J. B., and Cain, C. A. (**2008**). "Evolution of Bubble Clouds Induced by Pulsed Cavitational Ultrasound TherapyÂ¿Histotripsy," Ultrasonics, Ferroelectrics and Frequency Control, IEEE Transactions on **55**, 1122-1132.

[37] Wang, T.-y., Xu, Z., Winterroth, F., Hall, T. L., Fowlkes, J. B., Rothman, E. D., Roberts, W. W., and Cain, C. S. (**2009**). "Quantitative ultrasound backscatter for pulsed cavitational ultrasound therapy-histotripsy," Ultrasonics, Ferroelectrics and Frequency Control, IEEE Transactions on **56**, 995-1005.

[38] Flynn, H.G. and Church, C. C. **(1988)** "Transiet pulsations of small gas bubbles in water," J. Acoust. Soc. Am. **84,** 985-998.